REPORT DOCUMENTATION PAGE

AFRL-SR-BL-TR-01-

0318

1. REPORT DATE (DD-MM-YYYY)	2. REPORT TYPE	3. DATES COVERED (From - To)
06/04/2001	Final Report	Feb. 1997 - Sept. 2000

4. TITLE AND SUBTITLE
Turbulence and Complex Flow Phenomena in Axial Turbomachines

5a. CONTRACT NUMBER

5b. GRANT NUMBER
F496209710110

5c. PROGRAM ELEMENT NUMBER

5d. PROJECT NUMBER

5e. TASK NUMBER

5f. WORK UNIT NUMBER

6. AUTHOR(S)
Katz, Joseph and Meneveau, Charles

7. PERFORMING ORGANIZATION NAME(S) AND ADDRESS(ES)
The Johns Hopkins University
Department of Mechanical Engineering
3400 N. Charles St.
Baltimore, MD 21218

8. PERFORMING ORGANIZATION REPORT

9. SPONSORING / MONITORING AGENCY NAME(S) AND ADDRESS(ES)
Air Force Office of Scientific Research
801 North Randolph Street
Arlington VA, 22203-1977

10. SPONSOR/MONITOR'S ACRONYM(S)
AFOSR/NA

11. SPONSOR/MONITOR'S REPORT NUMBER(S)

12. DISTRIBUTION / AVAILABILITY STATEMENT

13. SUPPLEMENTARY NOTES

14. ABSTRACT
The objective of this project is to measure the flow within turbomachines, and use the data for addressing relevant turbulence-modeling issues. A unique two-stage, axial turbomachine test facility has been constructed. It contains liquid (66% NaI, 34% H_2O) with an optical index of refraction that matches that of the acrylic blades of the second stage. Consequently, it allows unobstructed view on the flow within the rotor, stator and the gap between them. Two and three dimensional velocity measurements can be performed using 2-D PIV and 3-D HPIV. The 2-D measurements are in progress and samples are provided. In the meanwhile we use PIV data generated in a centrifugal pump with a vaned diffuser to examine the flow at three modeling levels: Passage-averaged steady RANS, Unsteady RANS, and subgrid scale modeling for LES. Distributions of Reynolds, deterministic and SGS stresses within the impeller and the diffuser are determined and discussed. A new model is introduced for the deterministic stresses that accounts for interactions between the non-uniform outflux from one blade row with the neighboring blades. The model reproduces the correct magnitude of stresses occurring due to unsteady leading-edge separation in the diffuser.

15. SUBJECT TERMS
Particle Image Velocimetry, turbomachines, Deterministic Stresses, Turbulence

16. SECURITY CLASSIFICATION OF:			17. LIMITATION OF ABSTRACT	18. NUMBER OF PAGES	19a. NAME OF RESPONSIBLE PERSON
a. REPORT	b. ABSTRACT	c. THIS PAGE			19b. TELEPHONE NUMBER (include area code)
U	U	U	UU		410-516-5470

JOHNS HOPKINS
ENGINEERING

Department of Mechanical Engineering

G.W.C. Whiting School of Engineering
122 Latrobe Hall / 3400 N. Charles Street
Baltimore MD 21218-2686
(410) 516-7132 / FAX (410) 516-7254

Turbulence and Complex Flow Phenomena in Axial Turbomachines F496209710110

Final Report

to

Air Force Office of Scientific Research

Turbulence and Complex Flow Phenomena in Axial Turbomachines

Final Report

Submitted By

Joseph Katz and Charles Meneveau

Department of Mechanical Engineering
The Johns Hopkins University
Baltimore, MD 21218

This project was sponsored by the Air Force Office of Scientific Research under grant No. F496209710110. The program managers were J. McMichael and T. Beutner.

1.0 Executive summary

The objective of this project is to measure the unsteady flow in axial turbomachines and use the data to address turbulence and complex flow modeling issues that are specific to such complex environments. The research was funded under AFOSR grant #F49620-97-1-0110. This report has two sections. The first describes a unique two-stage axial-turbomachine flow visualization facility whose construction has been recently completed. This facility contains fluid (concentrated solution of NaI in water) with an optical index of refraction that matches that of the acrylic blades of the second stage. Consequently, it allows unobstructed view on an entire stage including the rotor, stator and the gaps between blade rows. Two and three dimensional velocity measurements can be performed using 2-D PIV (Particle Image Velocimetry) and 3-D HPIV (Holographic PIV). The 2-D PIV measurements are already in progress and sample data is provided. With available access to any desired plane (or volume), these measurements provide quantitative information on rotor-stator interactions, such as the effects of wakes on downstream blades, tip leakage flows and hub vortices and their interactions with neighboring blade rows, unsteady separation, particularly off-design conditions, etc.

In the second part of the report we examine turbulence and unsteady flow phenomena that have beenat three distinct levels of modeling: (i) Passage-averaged, steady RANS (Adamczyk, 1985), presently used for multiple blade-row simulations; (ii) Unsteady RANS, and (iii) subgrid scale (SGS) stress modeling for Large-Eddy-Simulation (LES). While the axial flow facility was under construction we have used 2-D PIV data obtained in a centrifugal pump with a vaned diffuser to address the various turbulence modeling issues. The results of this effort are presented in the PhD dissertation of Sinha (1999), and have already been published in several journal (Sinha et al., 2000a, b, 2001) and conference papers (Sinha et al., 1998a, b, 1999, 2000). We also introduce a new model of deterministic stresses for passage averaged RANS that accounts for interactions between the non-uniform outflux from one blade row with the complex blade geometry of the neighboring blades. Deterministic stresses calculated using this model are compared to measured distribution of deterministic stresses in the centrifugal pump. The model successfully reproduces the correct magnitude of deterministic stresses occurring due to unsteady leading-edge separation on the diffuser vanes. A paper describing this model has been submitted recently for journal publication (Meneveau and Katz, 2001).

The background and scientific objectives of this project are presented in Section 2. Section 3 describes the recently completed two-stage, axial turbomachine, flow visualization facility along with sample data. Section 4 presents the distributions of deterministic and Reynolds stresses obtained using the centrifugal pump data. These results have enabled us to develop analysis tools and explore modeling issues that are anticipated to arise in the new axial facility. Our effort to develop new models for deterministic stresses and comparisons to the available data are described in Section 5. Sample data SGS stress distributions and issues related to applications of LES in turbomachines are introduced in Section 6. Future plans are outlined in Section 7.

2.0 Objectives and Scientific Motivation

Flows in turbomachines, i.e. compressors, turbines, and pumps, are three-dimensional, complex and unsteady. These flow phenomena dominate the performance, efficiency, noise, and vibrations of these machines, and as a result must be understood and accurately predicted. The

scientific objectives are best understood within the context of modeling, as outlined in this Section. Tools for quantitative flow predictions in multi-stage turbomachinery have evolved considerably over the past few decades. Numerical simulation techniques are playing a role of growing significance in improving stage and overall efficiency during design, as well as in understanding complex flow-phenomena. An abbreviated list of these techniques is given below, in a sequence that roughly follows their chronology and their level of complexity.

2.1 Throughflow techniques: This steady, 2-D, 'traditional' simulation tool for multi-stage designs is based on solving axisymmetric problems, where the circumferential variations are averaged out (Adkins & Smith, 1982; Gallimore & Cumpsty, 1986). Non-axisymmetric effects have to be modeled using empirical correlations that account for blockage and mixing effects of blades, tip leakage, hub vortices and wakes. A concomitant problem of these models is that they work only near conditions for which they have been calibrated, typically near design conditions. While this approach is often complemented with limited, 2-D simulations of axisymmetric stream surfaces (or some single-stage 3-D calculations), it has difficulties dealing with three-dimensionalities and interactions between rows (see e.g. Dawes, 1992).

2.2 Passage-averaged 3-D Methods: This approach solves the steady, three-dimensional equations (Euler, or Reynolds-averaged Navier-Stokes -- RANS) separately in one (or a few) passage, in each of the blade rows of a multistage machine. Such steady 3D simulations are starting to be considered affordable for actual design purposes, even when a large number of stages is involved. Unsteady effects caused by neighboring rows are averaged out in the circumferential direction, and this information is passed along, from one row to another. There are basically two methods for transferring this information. The first is the "mixing plane approach" (e.g. Dawes, 1992; Denton, 1992), in which information is passed along as a boundary condition on a plane between blade rows. Although more accurate than through-flow techniques, it is very difficult to match all the parameters at the interface, resulting in discontinuities. The second and improved method is "the passage-averaged approach" (Adamczyk, 1985; Adamczyk et al., 1990; Rhie et al., 1998; LeJambre et al., 1998; Busby et al., 2000). Here the computational domain of a given row is extended to include the volume occupied by neighboring rows, but not the blades. The flow-turning effect associated with the blades (pressure difference across a surface) is introduced through steady body-forces, while the effects of the unsteady velocity field is introduced through "deterministic" stresses. This approach is more rigorous than the mixing plane method since it provides a framework for accounting for the effects of unsteady phenomena on the time averaged flow field. These effects cannot be accounted for by steady boundary conditions.

While the passage-averaged approach is very useful and affordable for design purposes, important modeling problems associated with unsteady interactions between blade-rows arise. In terms of modeling, in many current applications a frozen blade wake is swept through the field of the following row, and averaged. Consequently, unsteady interactions between blade rows are not accounted for. For example, in Sections 3 and 4 of this proposal we show how unsteady incidence angles resulting from the passage of rotor blades generate cyclic flow separations on the leading edge and mid sections of the stator blades (Sinha et al. 1999, 2000a, b). The rotor passage also alters the wakes of the diffuser vanes and the proximity to the stator vanes alters the structure of rotor wake. The effect of wake unsteadiness is considered in Adamczyk et al. (1996).

A deterministic stress model based on solving the unsteady Euler Equations (i.e. inviscid flow) has been recently introduced in Busby et al. (2000). Since the deterministic stresses are typically of similar or higher magnitude than the Reynolds stresses (see Section 4, Rhie et al., 1998, Le Jambre et al. 1998; Kirtley et al. 1993, and Sinha et al., 2000b), neglecting these interactions in simulations may lead to significant errors. Experimental data to determine these deterministic stresses is critical to guide and test new model developments. In the present project, we have generated such data at high spatial and temporal resolution, previously in the centrifugal facility, and in the future measurements, in the new axial facility (see Section 3). We also introduce another method to model the deterministic stresses, which compares favorably with the experimental data (see Section 5).

2.3 Phase-averaged unsteady RANS: This method involves two simulations of one or a few passages, one in the rotor frame and the other in the stator frame of reference. They are coupled by unsteady boundary conditions arising from sweeping the outlet plane of one solution past the inlet plane of the other (see e.g. Rai, 1987; Lakshminarayana, 1991; Survamshiya and Lakshminarayana, 1995, Ho and Lakshminarayana, 1995 and many others). This approach is currently limited to single-stage computations, since simulations of multi-stage configurations are prohibitive, especially when blade-counts vary from one stage to the next (complicating the phases that would have to be considered). Thus, it is understood that unsteady RANS of an entire multistage compressor is not on the horizon. This limitation justifies a continued interest in modeling issues of the passage-averaged technique. The usefulness of unsteady RANS in this context is in a way similar to the experimental data: It provides detailed data on the flow structure within a limited subsection of the turbomachine. The difficulty with unsteady RANS is the modeling of Reynolds stresses. Currently no consensus exists as to which of the many Reynolds stress models (simple k-ε, RNG-k-ε, second-order modeling, algebraic stress, low Reynolds-number corrections, etc.) is best suited for turbomachine applications (Lakshminarayana, 1991). Although modeling of unsteady RANS is not the primary focus of this project, still, as we have done with the centrifugal pump data, we will map the 2-D spatial and temporal distribution of the phase-averaged Reynolds stresses along with the unsteady flow structure. This data will be made available for code validation. We will also compare the Reynolds stresses to the deterministic stresses.

Turbulence modeling problems in unsteady RANS, especially in the complex environment of a turbomachine, create uncertainties associated with the validity of the results. The primary difficulties are caused by the fact that all the turbulence, including eddies with sizes comparable to an entire vane passage, must be modeled. Since these eddies do not have a universal structure (e.g. Wilcox, 1993; Speziale, 1991), it is necessary to adjust the models on a case-by-case basis, which reduces their effectiveness as a predictive tool. These difficulties have led to development of a wide variety of RANS models with varying complexity that are beyond the present scope. These models have led to significant improvements but not to breakthroughs. Consequently, to provide fundamentally more accurate simulations of turbulent flows in complex environment, it is of interest to explore the application of Large-Eddy simulations.

2.4 Large-Eddy-Simulation (LES): This approach does not average out random fluctuations associated to turbulence, but only smears out small-scale fluctuations (Rogallo & Moin, 1984, Lesieur & Metais, 1996; Meneveau & Katz, 2000). Spatially filtered, unsteady Navier-Stokes

equations (LES equations) are solved to capture not only the unsteadiness associated with relative motion between rotor and stator, but also to resolve random motion of large-scale turbulent eddies, such as large eddies in wakes, meandering of tip-leakage and hub vortices, etc.. Phase-averaged data is then determined by averaging the results. The spatial resolution does not need to approach viscous (Kolmogorov) length-scales because of the filtering. For now, a practical limitation of LES is that its computational cost is orders of magnitudes larger that RANS, mainly due to much longer integration times needed to achieve converged statistics. However, rapid increases in computer power are raising the expectation that LES may soon become practical even in complex turbomachine environments. More fundamentally, the filtering introduces "subgrid-scale" (SGS) stresses that account for the mixing and kinetic energy dissipation by the unresolved, small-scale fluctuations. Small-scale fluctuations in the inertial range of turbulence are known to be less flow dependent than the large-scale eddies, thus raising the hope for more "universal" models. There has already been considerable effort in development of LES models and applications to various basic flows, and some of increasing complexity.

Our group has experimentally examined several issues related to SGS modeling in relatively simple flows, such as homogeneous turbulence (Meneveau, 1994), the far-field of a round jet (Liu et al., 1994, 1995), in a cylinder wake (O'Neil & Meneveau, 1997), during rapid axisymmetric expansion (Liu et al., 1999), and within a square duct (Zhang et al., 1997, Tao et al., 1999, 2000, 2001). Considerable portion of this effort has involved implementation of PIV to generate the data-bases and some of the analysis has been based on hot wire data. The experiments and analysis in Tao et al. (1999, 2000, 2001) already involve use of HPIV to obtain full 3-D velocity distributions (130x130x130 vectors) in a finite volume (4.5x4.5x4.5 cm^3). These data are filtered at different spatial scales, which allows us to compare between large (resolved scales) and small scales (subgrid stresses). As reviewed in Meneveau & Katz (2000), the basic modeling paradigm that has been established by our work is the use of computed large-scales to locally guide the modeling at small scales. We learned from simpler flows that model coefficients must be modified when turbulence is exposed, for example, to rapid straining or when the filter scale approaches the integral scale. The available data indicates that such modifications can be determined from the response of the resolved structures to the local flow. LES, unlike RANS, allows us to perform "dynamic" modifications to the modeling, since part of the turbulence is resolved. When applying LES to the unsteady flow in a blade-passage, there is a need to implement much more refined models to account for different flow regimes.

As described in Sinha et al., (1998a, b; 1999, 2000a, b) and summarized in Section 6, we have used PIV data in a centrifugal pump with a vaned diffuser to directly measure the relevant large-scale, filtered flow structure, the distribution of subgrid-scale stresses and the associated kinetic energy dissipation. Interesting phenomena, such as regions with consistent energy backscatter (from small scales to large scales) have been identified. We also find, consistent with results from simple geometies, that eddy-viscosity models are inherently deficient. Filtering of the data at various scales (provided the data has sufficient resolution) should enable us to compare the response of different scales to the external forcing, and incorporate the measured behavior into improved modeling. We plan to perform these measurements in the new axial flow facility described in the next section.

3. Axial Flow Facility

3.1 Rationale for the Selected System: Providing answers to the various levels of modeling problems outlined in section 2, specifically those of deterministic stresses for passage-averaged formulations and subgrid-scale stresses for LES, requires data with high spatial and temporal resolution. Furthermore, the data set must be complete, i.e. it should cover the entire flow structure within a blade passage, including hub vortices, tip region, wake structure, boundary layers on the blades, etc.. To generate such data, using optical techniques one needs unobstructed view of the entire domain, at any phase angle. Also, since all optical techniques involve measurement of motion of tracers, they must be uniformly distributed in the flow-field, including the powerful vortical structures associated with tip-leakage flows. These requirements dictate the kind of facility and experimental method that is available to us at this time. The need to observe the entire flow field in fine detail requires the use of PIV (and HPIV), a method with which we have considerable experience of applications in complex geometries, including pumps (e.g. Dong et al., 1992a, b, 1997a, b; Chu et al., 1995a, b; Sinha et al., 1998a, b, 1999, 2000a, b; Roth et al., 1999, 2001). The few other applications of PIV to flow in axial turbomachines have been severely limited by optical access and reflection problems (Bryanston-Cross et al., 1992; Tisserant & Breugelmans, 1995).

Access to the entire flow domain at any phase angle can be achieved by using a fluid and blade made of material with the same optical index of refraction. Such an arrangement would enable us to resolve the flow between the blade tip and the casing, and within boundary layers. Use of neutrally buoyant particles prevents problems involved in seeding strong vortices, by preventing relative motion caused by centrifugal forces. Thus, the chosen facility for dealing with the problems outlined above contains liquid seeded with neutrally buoyant particles with transparent blades made with material of the same index of refraction as the fluid. The resulting facility, that has been under construction for the past three years (details follow) and has been completed recently, consists of a two-stage axial pump (rotor, stator, rotor, stator), with blade-shapes that are characteristic to aircraft compressors. At this time, the favorable test conditions afforded by index matching and neutrally-buoyant particles cannot be achieved using air facilities. The shortcoming of our experimental conditions is lack of compressibility and temperature variation effects. Consequently, the flow structure is substantially different from conditions that are encountered in the first stages of high-speed compressors, where shocks dominate the flow (see e.g. Copenhaver et al., 1996). However, to answer the turbulence modeling questions raised in the previous section, it is more important to obtain full and detailed data, even if it is only relevant to the predominantly subsonic portions, such as the aft stages of compressors.

2.2 Detailed Description of the New Facility: The recently completed test facility allows detailed measurements of the velocity distribution within an entire stage, including the rotor, stator, gap between them, inflow into the rotor and the wake downstream of the stator. Sketches of the system are presented in Figures 1 - 3. Figure 1a is an overall view of the test loop. Figure 1b provides details on the pump, support structure, drive system, windows, etc., and Figure 1c shows the rotor and the stator. The location of the two windows relative to the blade rows, are presented in Figure 2a and dimensions are provided in Figure 2b. Several objectives are met by this design. First, this setup provides a realistic representation for flow conditions in multi-stage axial turbomachines (excluding compressibility effects) including realistic blade geometries,

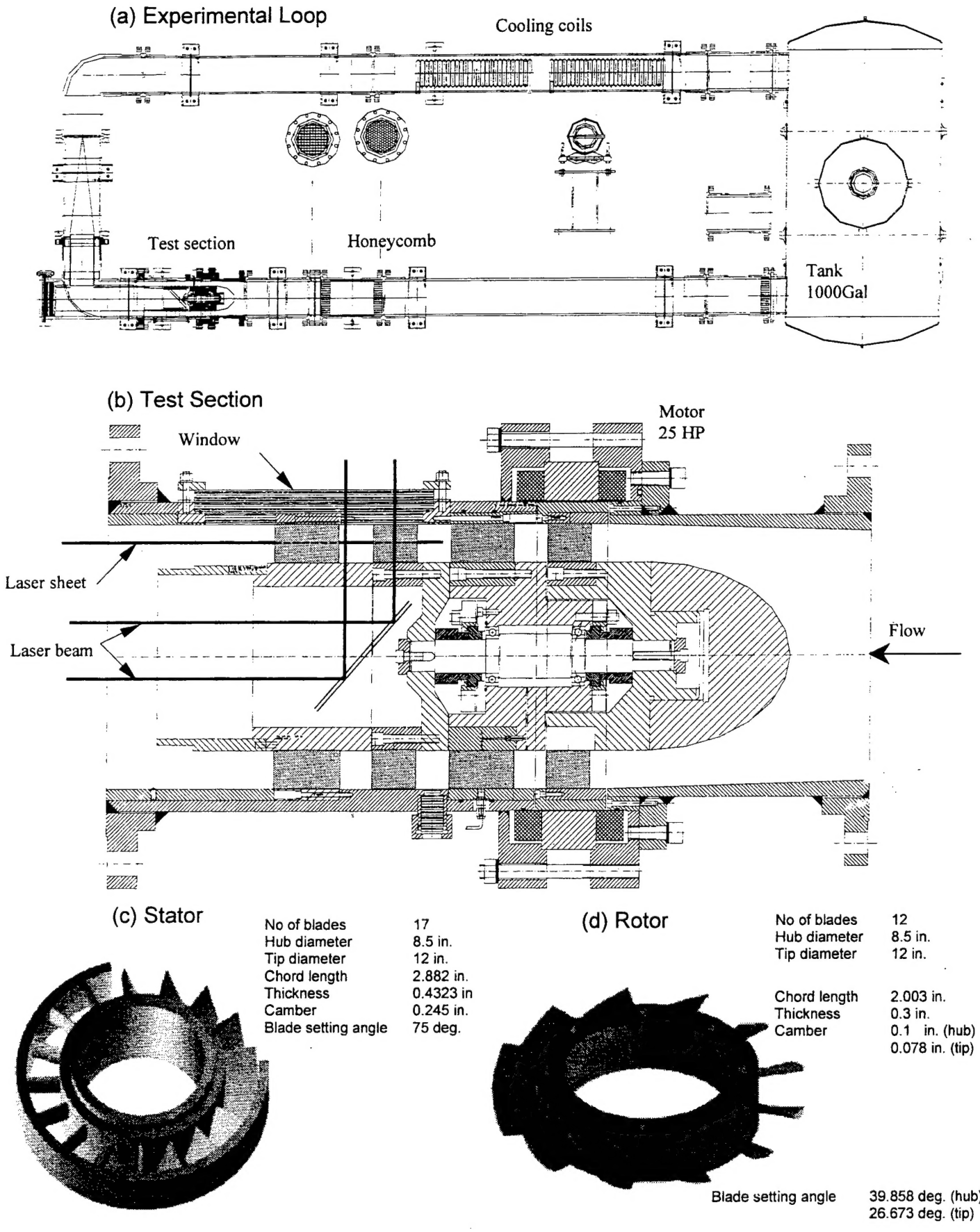

Figure 1: The recently completed, two-stage axial turbomachine flow facility: (a) overall view of the test loop; (b) close-up layout of the motor, 4 blade rows & bearings; (c) stator; and (d) rotor.

Figure 2: (a) A close-up drawing of the recently completed two-stage turbomachine, showing the location of windows and corner setup; (b) The present set of four blade rows with dimensions. The distance between rows of the second stage can be adjusted.

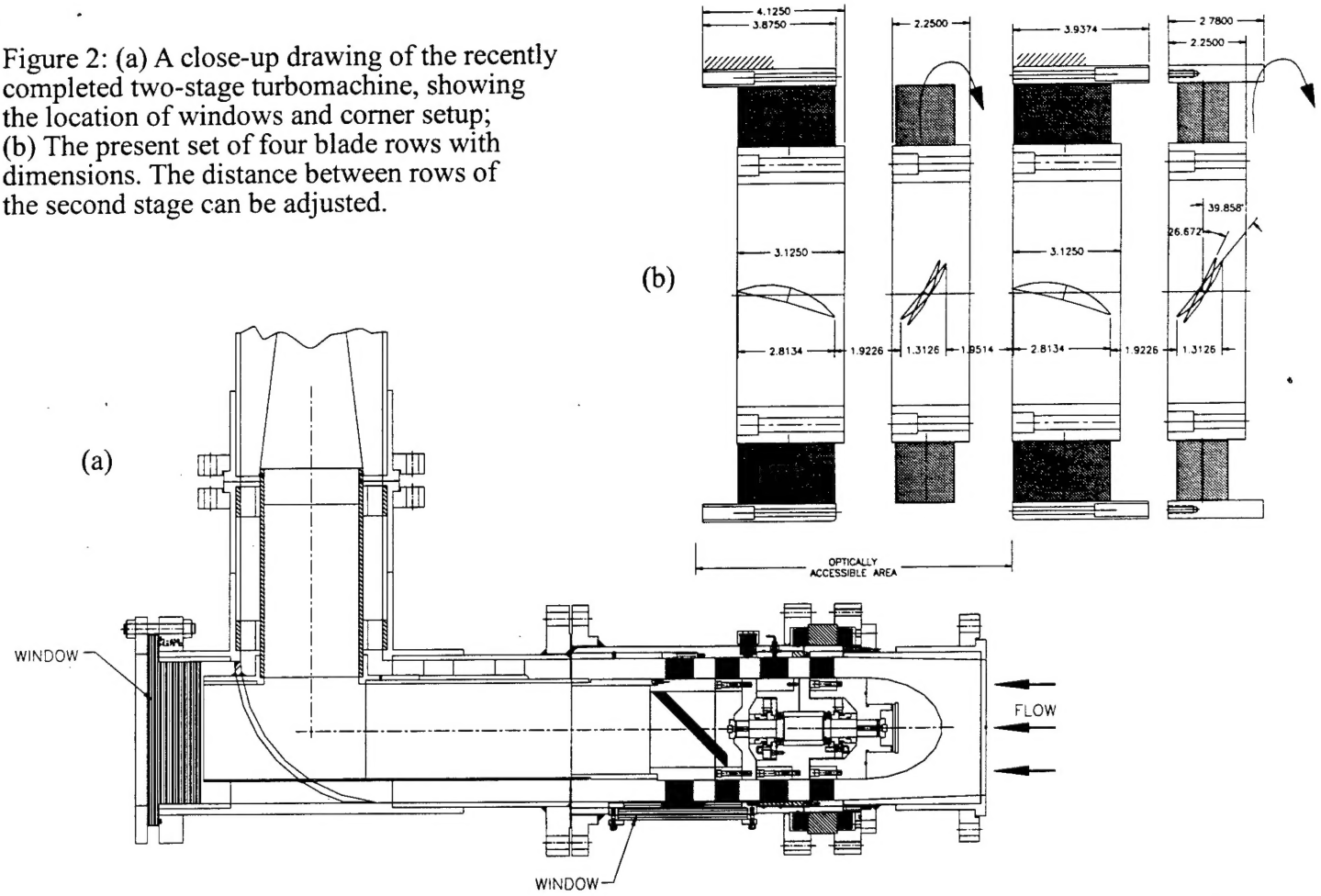

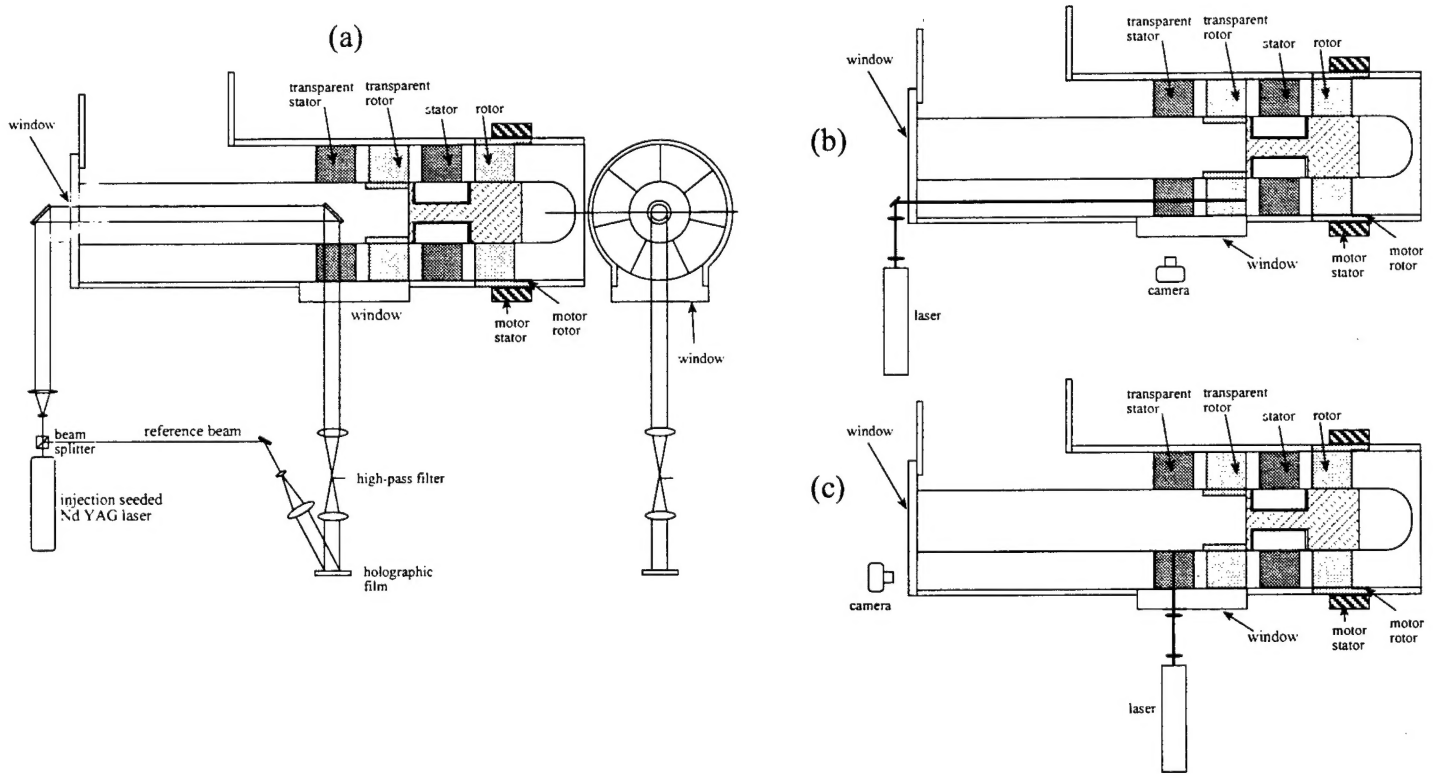

Figure 3: The optical seup for velocity measurements in the new axial pump facility. The pump geomtery is simplified in order to illustrate the optical elments. (a) The holographic PIV setup; (b) The 2 - D PIV setup for measurements in a plane parallel to the pump axis; (c) 2 - D PIV setup for measurements in a plane notmal to the pump axis.

high Reynolds numbers and closely spaced blades that characterize aircraft compressors. Second, it provides unobstructed view for 2-D PIV and 3–D holographic PIV measurements within the entire second stage, including the boundary layers on the blades, the flow around the hub and the tip leakage region. Funding for constructing this facility has been provided both by AFOSR (to deal with the modeling problems outlined in Section 2) and by ONR (to study stability, gust response and hydro-acoustics of swirling flows using different blade geometries than those shown in the present report).

The test loop (Figure 1a) consists of a 4 m^3 tank and 12" diameter pipes that contain means for generating and reducing the free stream turbulence (as required) as well as for controlling the temperature. The test section is located near one of the corners. This two - stage axial turbomachine consists of four blade rows. The two rotors have a common shaft that is supported by precision bearings immersed in a sealed oil bath. All the blade rows have an outside diameter of 30 cm and a hub diameter of 21.6 cm. The design flow rate is 3000 gpm (0.195 m^3/s) and the total pressure rise in design conditions is about 66 kPa. The system is driven at 900 rpm (maximum speed) by a 25 HP rim-driven, permanent magnet, AC motor. The rotor of the motor is encapsulated in a stainless steel shell and is directly connected to the band surrounding the rotor of the first stage. The second stage is driven by the common shaft. This drive mechanism has several advantages. First, since the system does not have a long shaft leading to an external motor it allows unobstructed illumination from the back side of any point in the second stage (details follow). Second, the direct connection to the first blade row, short hard shaft and precision bearings insure quiet and reliable operation with minimum vibrations. Indeed, recent tests performed with the completed system confirm that the system operates at very low level of noise and vibrations.

The structure containing the bearings is held in place by the first stator. The first stage is made of metal (Naval Bronze) and the entire second stage (rotor, stator and hub) is made of acrylic. To avoid undesirable secondary flows and massive separation the 21.6 cm diameter hub extends around the corner (Figure 2a) and then tapers slowly at a cone angle of 7^0. The 12" pipes are divided to several sections that enable us to insert honeycombs and screens for reducing the turbulence as well as grids for generating turbulence. Both rotors have 12 blades, each with a chordlength of 50 mm, span of 44.5 mm, thickness of 7.62 mm and camber varying between 2.54 mm at the hub to 1.98 at the tip. The stators have 17 blades, each with a chordlength of 73.2 mm, span of 44.5 mm, thickness of 11 mm and camber of 6.223 mm. The blade rows were manufactured using precision CNC machines and the surfaces were subsequently hand finished to maintain the surface roughness below 0.0076 mm. The test loop has a temperature control system and provides considerable flexibility in installing other devices including pressure transducers, honeycombs and grids as well as changing blade rows.

The entire system, as shown, is now operational. A recently awarded AFOSR DURIP grant provided (among other items that will be described later) the funds for installing an in-house-designed "torturous-path valve" in the test loop. It will enable us to match the pressure drop in the loop to the desired (on or off-design) conditions of the pump, without the adverse effects (massive flow separation) of commercial valves. This valve will be designed, manufactured and installed in the coming year.

3.2 Optical Access: Optical access is provided by a window that extends from upstream of the rotor, covers the entire second stage and terminates downstream of the stator (Figures 1b & 2a). In addition, a large window located at the corner of the facility provides an unobstructed view in the axial direction. As illustrated in Figure 3b - c, these windows enable us to illuminate any desired plane with a laser sheet (for 2-D PIV measurements), from the hub to the tip of the blades. The interrogated planes can be parallel or normal to the axis of the pump. The corner window also provides us with an optical access to the interior of the rotor and the stator, which is essential for 3-D, holographic PIV measurements. The optical setup for HPIV is presented in Figure 3a. It is based on a system that has been developed and implemented in our laboratory for the past several years (Zhang et al., 1997; Tao et al. 1999, 2000, 2001). As described in these references, HPIV presently enables us to record and generate an array of 128x128x128 instantaneous velocity vectors.

In order to provide unobstructed view of the flow near curved and skewed blades (and transmission of the laser sheet through blades), especially close to the hub and the tip, we use a fluid that has an index of refraction equal to that of the acrylic blades and window. Based on initial tests we opted to use water with concentrated (66% by weight) solution of NaI. This fluid has a specific gravity of 1.85 and a kinematic viscosity of $1.08X10^{-6}$ m^2/s (i.e. very close to that of water). The resulting Reynolds number based on the tip speed and rotor chordlength is $6.1x10^5$. With this index-matched fluid the entire second stage becomes invisible, providing an unobstructed view of any point. Matching the index of the hub and the window also allows unobstructed transmission of the illuminating beam of the holography system (Figure 3a). The cost of the NaI is substantial - $28,000-$30,000 to fill the entire facility. About half of the funds for the salt have been provided by an AFOSR DURIP grant (mentioned above) and the other half was provided by ONR funding. The salt has already been mixed with the water and the facility has operated with the index-matched fluid for several months with little difficulties. One of the difficulties that we had to overcome is the tendency of a small fraction of the I^- ions to be oxidized into I_3^- once it is exposed to light and to Oxygen. The latter absorbs green light, which complicates the PIV measurements. Experiment and testing using spectroscopy showed that limiting the exposure of the water to light, and maintaining an oxygen-free environment within the facility (the tank with the water-gas interface contains pure nitrogen) solves this problem. We did not detect any significant levels of I_3^- in the water for several months.

All of the optical elements shown in Figure 3 already exist and have been integrated with the test facility. The injection seeded Nd-YAG laser has been purchased using funds provided by a 1996 AFOSR DURIP grant. A recently awarded AFOSR DURIP grant provided the resources for purchasing a high resolution (2K x 2K $pixels^2$) "cross correlation" digital camera and data acquisition system with a special "buffer memory" feature (interline transfer) that enables recording of two frames with very short delays between exposures (2 μs). It overcomes the shortcomings of an existing 2kx2k camera (Sinha et al., 2000a, b) that has a realistic minimum delay between exposures of 50μs, which severely limits its ability to record data in the high-speed flows expected in the turbomachinery facility. It also overcomes the resolution limitation of our 1K x 1K camera, which is critical when the data is spatially filtered in order to determine the SGS stresses for LES. The new 2Kx2K camera has already been purchased and integrated with a high-speed image acquisition system. Data at 60 MB/s can either be stored on a computer RAM or sent directly to a hard disk. The laser and data acquisition system are also integrated

with the control system of the test facility that receives a signal from a precision shaft encoder. A delay generator enables us to record data at any desired phase of the rotor.

We have also measured the velocity distributions at the inlet to the first stage. The mean flow appears as a classical turbulent pipe flow without any significant distortions. The performance curve of the pump has the desired/expected trends. With minimum disturbances in the loop (except for honeycombs) the total flow rate reaches the expected value of 019 m^3/s (3000 gpm) and a pressure rise of 65 KPa. Well below design conditions the familiar signs of stall appear, which may be used in the future for studying the flow structure in a stalled pump, as we have done in the centrifugal facility (Sinha and Katz, 1999; Sinha et al., 2001).

3.*3 Preliminary Results:* Measurements of the flow structure and turbulence around the rotor and stator blades are currently in progress. Sample images and velocity distributions in the axial flow facility are presented in Figures 4-7. Figure 4a is a superposition of images with the impeller located at 10 at different positions. The flow is illuminated by a single light sheet from the left and the (white and red) traces are the intersections of the sheet with the rotor and stator blades at 10 different phases. As is evident, the same sheet penetrates through blades and maintains its shape. The slight variations in beam intensity, which occur due to very small differences in refractive index, do not have significant effects on the quality of the PIV images. They disappear after image enhancement and we can obtain a complete data set over the entire flow field.

A sample enhanced PIV image (one of the two exposures) near the trailing edge of the rotor is presented in Figure 4b. Mean velocity distributions near the rotor blade trailing edge in absolute and relative frames are presented in Figure 5. The blade wake is clearly evident. The flow around the leading edge of the rotor is presented in Figure 6 and a phase-averaged flow near the leading edge of the stator is presented in Figure 7. Phase averaging implies that all the data is recorded at the same rotor orientation. Flow non-uniformities caused by the rotor wake are clearly evident upstream of the stator. We are presently in the process of recording an extensive data base of the entire flow field at 10 different rotor phases. About 100 instantaneous velocity distributions are required for obtaining a converged mean distribution. About 1000 instantaneous distributions are required for obtaining converged statistics of the turbulence parameters. Examples of older data and obtained in the centrifugal pump facility and how it is used for addressing turbulence modeling issues are presented in the following Section.

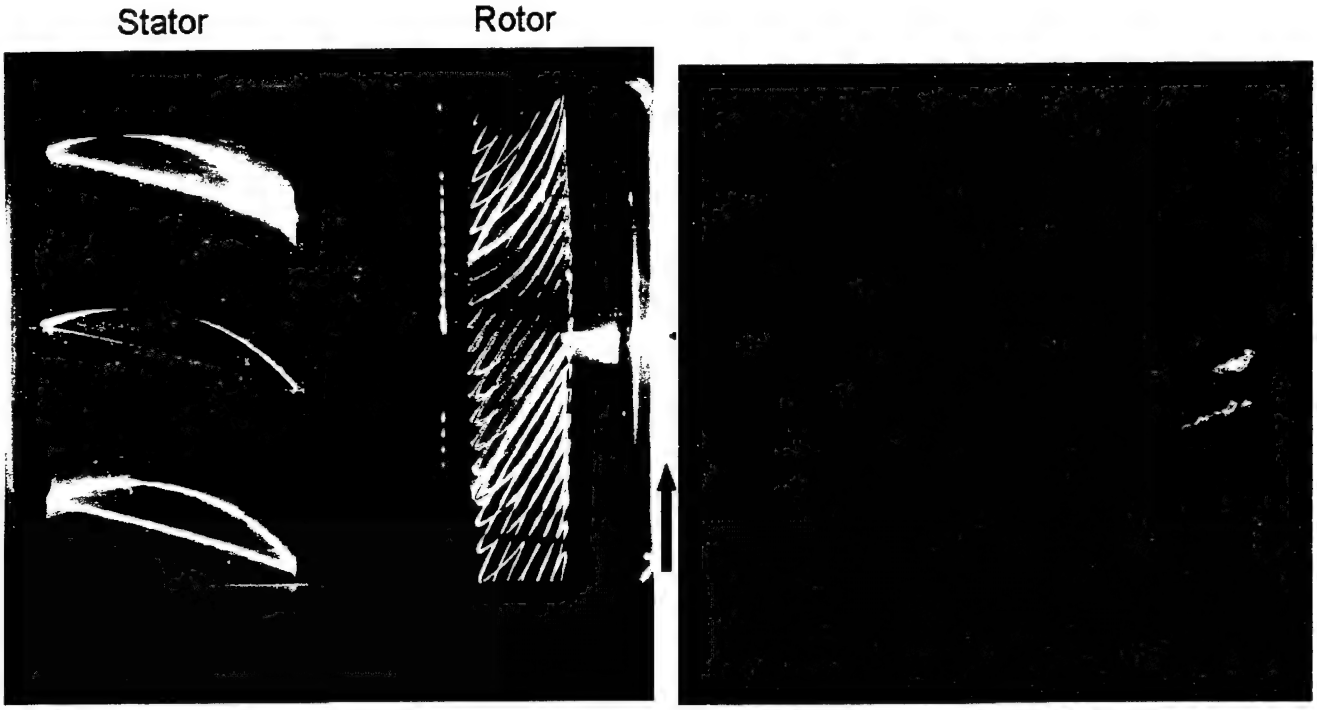

Figure 4: a. A superposition of 10 images at different rotor phases showing stator (on the left) and rotor blades (on the right) illuminated from the left by the same laser sheet. The ten locations of the same rotor blade are marked in red. Note that there is no obstruction to the field of view anywhere in the flow field. The small variations in beam intensity occur due to slight differences in refractive index. They disappear after enhancement do not affect our ability to obtain high quality data there (see Figure 7 below). An enhanced PIV image (only one exposure) of the flow near the trailing edge of the rotor.

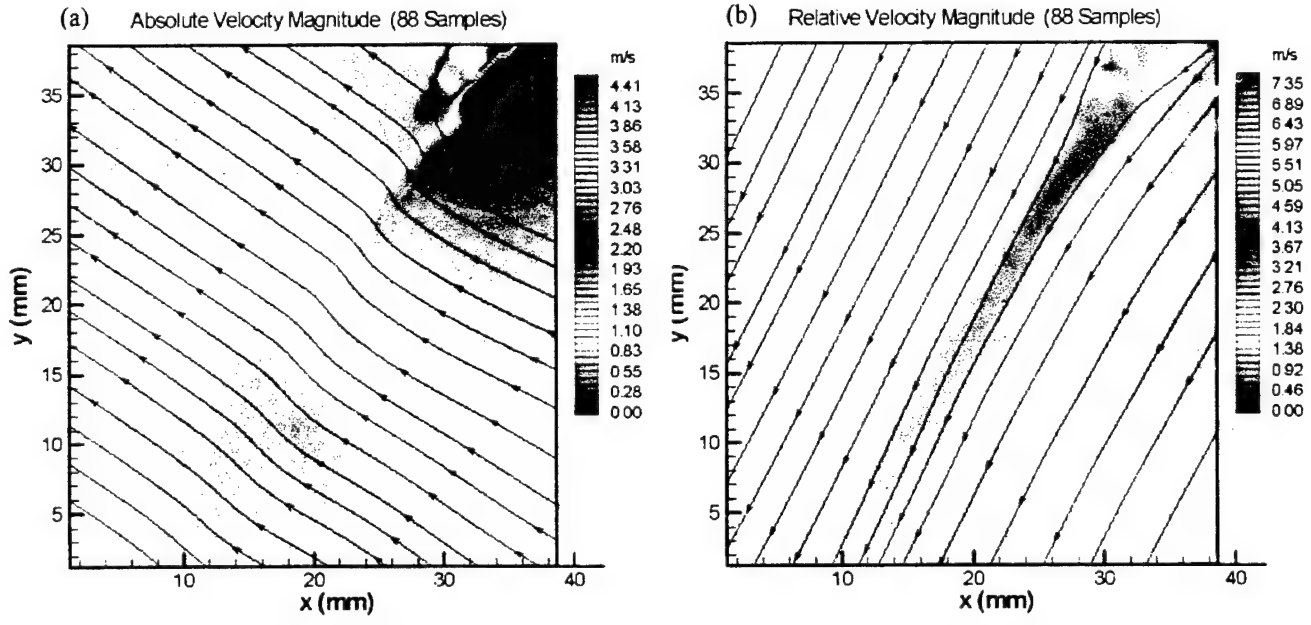

Figure 5: Sample absolute (a) and relative (b) mean velocity distributions along with streamlines at the trailing edge of the rotor.

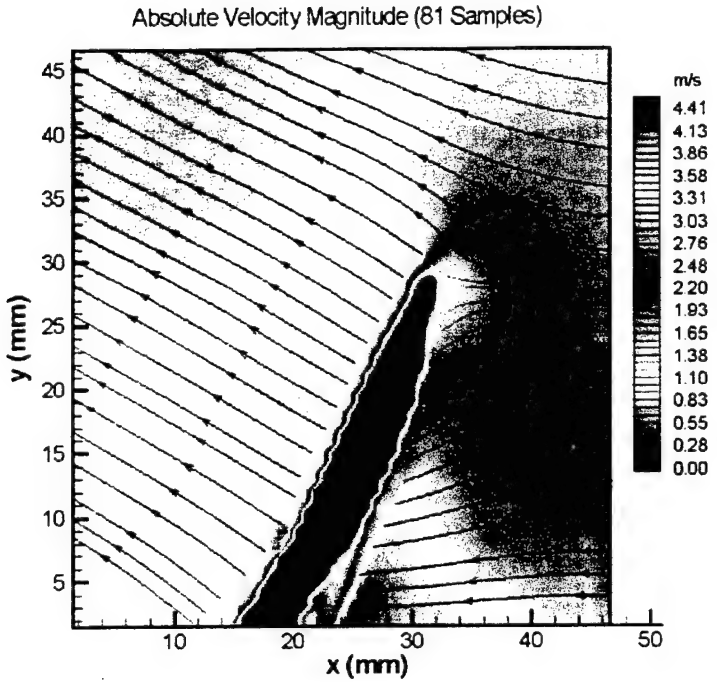

Figure 6: Sample absolute mean velocity distribution along with streamlines in the vicinity of the leading edge of the rotor blade. Note that the velocity is measured on both sides of the blade simultaneously.

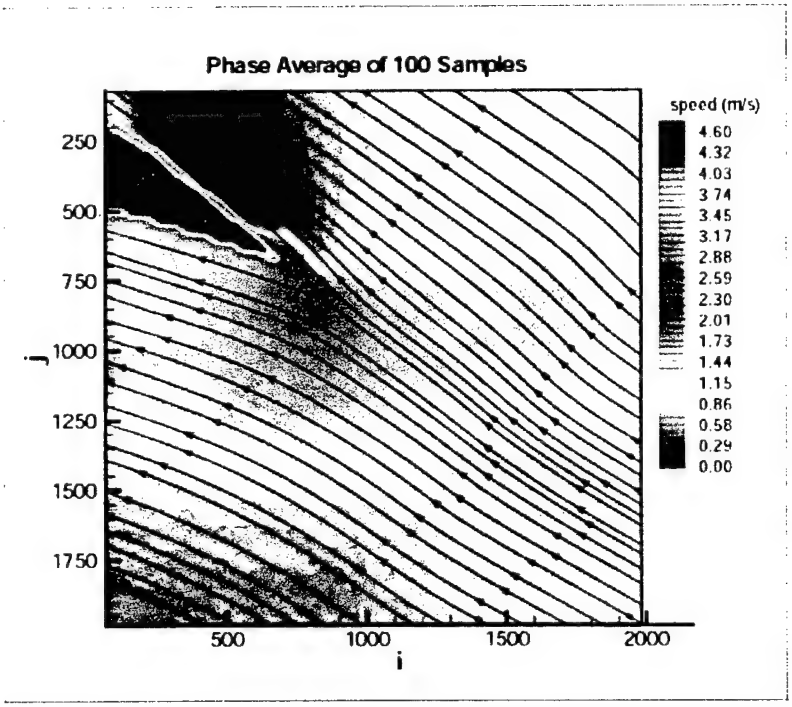

Figure 7: The phase-averaged (same rotor phase) mean velocity distribution along with streamlines near the leading edge of the stator blade. The flow field is illuminated from behind (Left side).

4. **Measurements of Deterministic, Reynolds and SGS Stresses Using Data Obtained in A Centrifugal Pump With A Vaned Diffuser.**

While the axial flow facility described in Section 3 was under construction we used available PIV data generated earlier in our centrifugal pump facility to measure and compare the Reynolds as well as deterministic stresses associated with rotor-stator interactions. Issues arising in LES modeling have also been examined. The actual experiments in the centrifugal facility have been funded by ONR with objectives related to hydro-acoustics, providing data for RANS code validation, as well as the flow structure and associated pressure fluctuations of a stalled pump, well below design conditions. In this section we describe the facility very briefly, and present only results of data processing, analysis and modeling that are directly relevant and have been supported (at least in part) by AFOSR. Included are processed and analyzed data (as well as procedures) that are related to turbulence modeling at the different modeling levels indicated in Section 2. Detailed information on the facility, flow structure in the pump when it operates on design conditions (including the turbulence modeling issues) and during stall are described in Sinha et al. (1998a, b; 1999; 2000a, b, c, 2001).

4.1. Centrifugal Pump facility and Data Acquisition: The experiments were performed in a transparent centrifugal pump with a vaned diffuser that enables PIV measurements within the impeller (rotor), the gap between the rotor and the stator, within the diffuser vanes passages and in the volute. The test loop has been used in previous studies (e.g. Dong et al., 1992a, b, 1997, Chu et al., 1995a, b) but the pump is new. As shown in Figure 8a, the impeller has five backward swept blades with a logarithmic profile, each with an exit angle of 21.3^0. The inlet and blade tip diameters of the impeller are 8.51 and 20.32 cm, respectively. The diffuser has 9 blades with inside and discharge diameters of 24.45 cm and 30.5 cm, respectively. The circular arc vanes have a chord length of 13.44 cm, inlet and exit angles of 10.6^0 and 10.97^0, respectively, and a span of 1.27 cm. The pump is operating at design conditions at 890 rpm. The PIV system utilizes an Nd-YAG laser and the images are recorded on a 2048x2048 pixels^2, 4 frames/sec, digital camera equipped with hardware based image-shifting capability. This camera provides excellent image quality and resolution for PIV. However, as noted before, limitations in the speed of image shifting limits its application in high speed, high-magnification, bi-directional flows expected in the axial facility where we have adapted a new 2Kx2K cross-correlation camera purchased under AFOSR DURIP grant. Neutrally buoyant, ~30 μm diameter, fluorescent particles (manufactured in-house) are used as tracers.

4.2. Sample Results: Comparison of Deterministic stresses and Reynolds stresses: In order to compare the turbulent and deterministic stresses we measured the phase averaged velocity distributions at five different impeller blade orientations by averaging 100 instantaneous distributions at each phase. The rms values of velocity fluctuations were determined from the difference between the instantaneous and phase averaged data. This process generated five substantially different distributions of turbulence parameters. The turbulent kinetic energy, k^*, was estimated by summing the two measured normal stresses and multiplying the result by 3/4, in order to compensate for the (out of plane) missing component.

To estimate the deterministic kinetic energy in the stator frame of reference we first determine the passage-averaged velocity (Figure 8b) by averaging the phase-averaged velocity fields. To

obtain unbiased data we added additional phase averaged distributions, every ten degrees (with interpolated values between them) that completed an impeller blade cycle of 72 degrees (there are 5 impeller blades). The deterministic stresses were estimated from the differences between the phase-averaged and passage-averaged data. The deterministic kinetic energy, k^{*det}, was estimated by summing the normal stresses, again multiplied by the same 3/4 factor. Figures 8c and 8d compare the distributions of k^{*det} to k^* at one of the five phases for which the Reynolds stresses were determined (Sinha and Katz, 2000a contains the rest).

As is evident from these samples, k^{*det} is high within the impeller, at the pressure and suction sides of the diffuser vane and in the wake of the diffuser. It peaks at the leading edge of the vane, where the phase-averaged flow separates intermittently (not in the conditions shown in Figure 8c). This separation occurs as the incidence angle at the entrance to the passage increases substantially as the entrance to the vane passage faces the pressure side of the impeller blade ("jet – wake" phenomenon – see below). Another form of phase-dependent flow separation occurs on the same suction side (convex side) of the vane, near the point that lines up with the trailing edge of the previous vane. It occurs as the entrance to the passage faces the suction side of the impeller blade (i.e. the orientation shown in the example) because of the reduction in total pressure at the entrance to the passage. High values of k^{*det} in the wake of the diffuser indicate that the flow there is also phase dependent. *Clearly, the results demonstrate that the highest deterministic stresses are associated with interaction of the non-uniform flow at the exit from the impeller with the boundary layers on the diffuser vanes.* A model for the deterministic stresses consisting of a sweeping wake (e.g. Rhie et al.,1998) will miss essentially all of these phenomena. k^{*det} is also very high within the impeller due to internal flow non-uniformities, typically referred to as the "jet – wake" phenomenon (Dean & Senoo, 1960). It consists of a higher radial velocity on the pressure side of the impeller blade and low in the suction side, and conversely, high circumferential velocity in the suction side and low in the pressure side. These non-uniformities occur in addition to the viscous wake of the impeller and in the present flow they are dominant.

In the regions with concentrated k^{*det}, the magnitudes are considerably higher (up to three times) than the turbulent stresses (note the differences in scales). The turbulent stresses are high in the wake of the impeller blade, along the walls of the diffuser vanes and in the wake of the vanes. In the gap between the diffuser and the impeller the distributions of k^* show wakes of vanes located outside (above) of the sample area. The left side of Figure 8c shows elevated turbulence generated by a vane located 80^0 (almost 1/4 diffuser) upstream of the sample area. Thus, the entire volute consists of a series of wakes generated by the impeller blades and diffuser vanes. The separation phenomena mentioned above impact the turbulence along the suction side of the vane. In the example shown, one can see the effect of mid-chord separation (the leading edge separation occurs at a different phase).

As discussed in Sinha at al. (2000b), although in some cases, such as in wakes, one finds peaks of deterministic and Reynolds stresses at the same location, in general the trends of k^{*det} are considerably different than those of k^*. Thus, different modeling approaches must be used. Such modeling is a primary objective of this study.

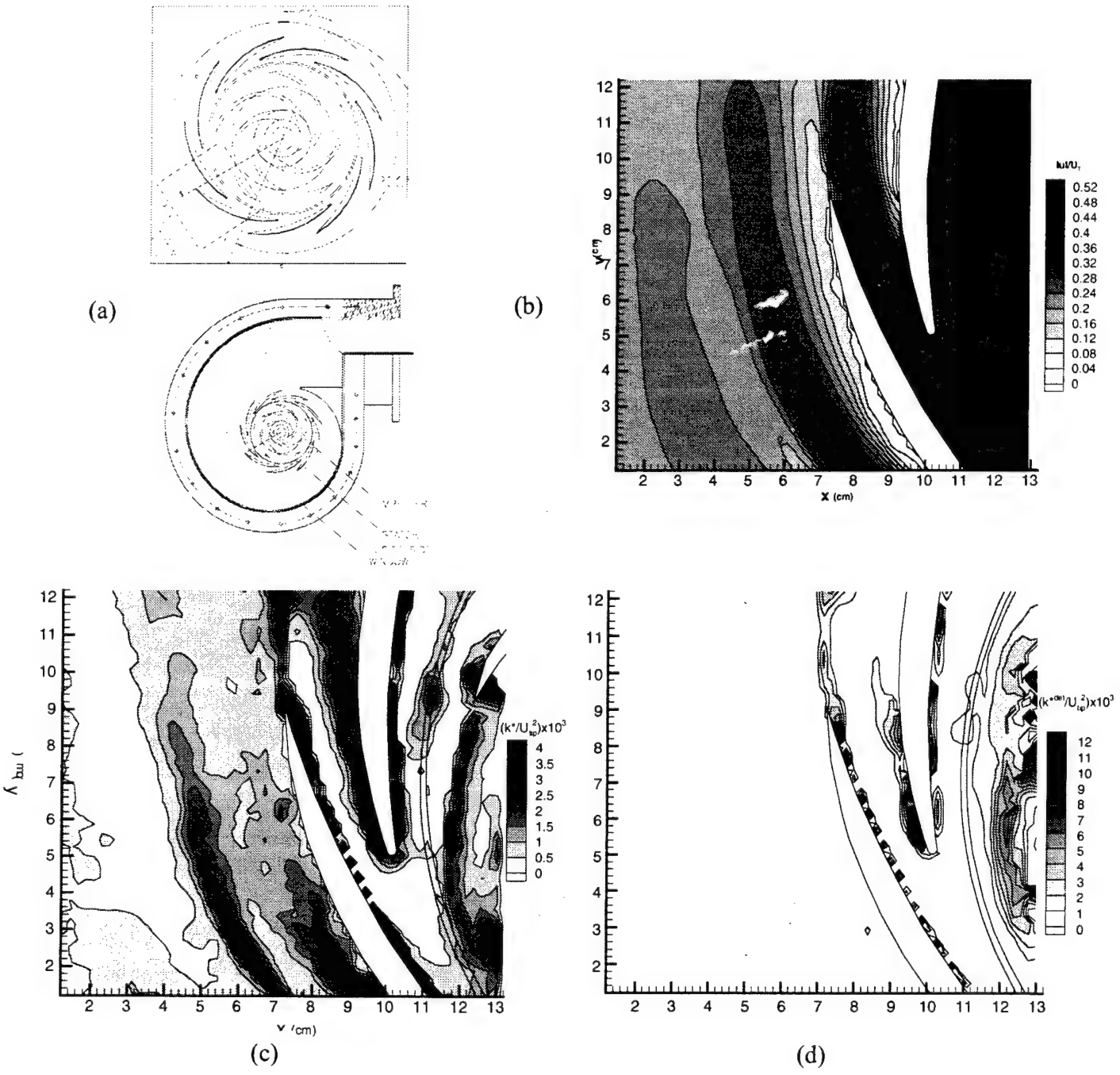

Figure 4: (a) The geometry of the centrifugal pump facility with a vaned diffuser showing the location of the sample area; (b) Passage-averaged velocity in the diffuser frame of reference, obtained by averaging over all possible phase-averaged distributions (phase is based on the impeller blade orientations); (c) Sample distribution of turbulent kinetic energy, k^*, (one of five available) when the impeller blade is located at $\theta=246^0$. Note the wake of the impeller blade, the wakes of the diffuser vanes and the high turbulence along the suction (convex) side of the vane; (d) distribution of deterministic kinetic energy, k^{*det}. Note the differences in scales and the high deterministic energy near the leading edge of the vane, in the wake of the vane and in the area occupied by the impeller.

Determination of the passage-averaged velocity and stresses in the rotor frame of reference is more complicated since we need to rotate the measured velocity field of different phases and match the location of the impeller blade. In order to obtain data over a domain that covers at least one vane passage, the rotated velocity field must be substantially larger. To generate this data we patch two flow fields of the same domain that are recorded at different impeller phases, as illustrated in Figure 9a. A series of five such pairs along with interpolated fields are then rotated and aligned such that the impeller blade is located in the same place. The rotor passage-averaged velocity distribution (Fig. 9b) clearly shows the wake of the blade. The highest deterministic stresses (Fig. 5c) occur in the domain occupied by the diffuser vanes that have been passage-averaged out. However, high deterministic stresses occur also in the wake of the impeller. This effect is caused by meandering of the wake due to the circumferential non-uniformities of the pressure distribution upstream of the diffuser vanes. Thus, "potential flow" effects, that depend on downstream conditions and are not associated with wakes, contribute substantially to the deterministic stress.

In the following section we use the measured distributions of deterministic stresses (in the stator frame of reference) and their dependence on the jet-wake phenomenon to introduce a methodology for modeling the deterministic stresses.

5. **Bimodal deterministic stress model:**

5.1 Basic Idea and Experimental Validation: As noted before, the model introduced in this chapter is described in detail in a paper that has been recently submitted for publication (Meneveau and Katz, 2001). The measured deterministic stresses presented in Section 4 show strong tangential variations which by construction are not included in the "swept wake" model of Adamczyk et al. (1990). In that model the wake profile resulting from the steady calculation in the preceding blade row is swept circumferentially over the domain, and deviations from the mean velocity are averaged over the tangential direction to calculate the modeled deterministic stresses. This averaging process eliminates any tangential variations of the resulting stress field. Conversely, a substantial part of the real deterministic stress field is caused by the unsteady response of the flow around the stator blades, particularly the boundary layers and the wakes, to non-uniform pressure and velocity distributions at the exit of the impeller. Hence, improved models that account for rotor-stator interactions are needed. These observations provide the motivation for developing the presently proposed bimodal deterministic stress model, which is described below.

The proposed model only accounts for the cyclic contributions to the deterministic stresses, and neglects the effects of "passage-to-passage" variability (see Adamczyk et al., 1990). This model is based on the expectation that the phase-averaged, time-varying outflow from a blade row is reasonably well correlated with sweeping an accurately computed passage-averaged outflow from the same blade row (computed in the frame of reference of this blade row). The following example will clarify this point. Specifically for the centrifugal pump discussed in Section 4, Figure 10a shows the measured angle α between the velocity at a point P (P is shown in Figure 6b) and the circumferential direction, as function of rotor orientation angle θ (the frame of reference is defined in Figure 8a). The solid circles show α obtained form the measured phase-averaged velocity fields at various rotor orientations. A jet-wake like phenomenon is evident: For $\theta < 210^0$, i.e. when point P is in the pressure side of the impeller blade, the radial velocity at the

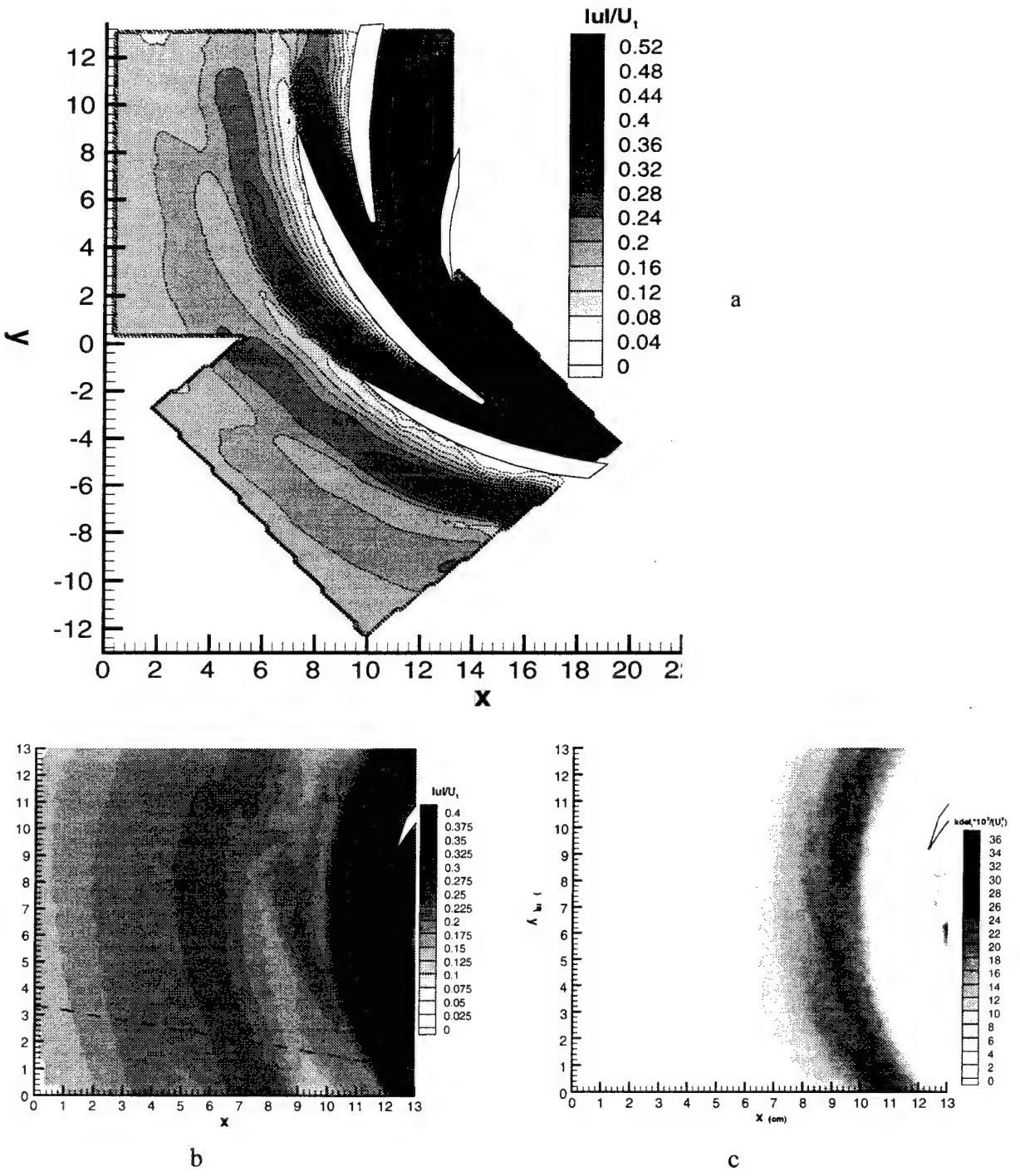

Figure 5: (a) a matched pair of phased averaged velocity distributions. A series of such pairs is used for determining passage-averaged velocity distribution in the rotor frame of reference;
(b) passage averaged velocity distribution in the rotor frame of reference (averaged over all possible stator orientations). For clarity and for highlighting the local variations, ωr is subtracted from each vector; (c) distribution of deterministic kinetic energy in the rotor frame of reference. Note the high kinetic energy in the wake of the impeller.

exit from the rotor increases and the circumferential velocity decreases. Consequently, the angle of incidence of the flow at the entrance to the stator blade row increases, as compared to the lower angle during the rest of the cycle. As discussed before (and in Sinha et al. 2000a, b) this incidence angle change causes phase-dependent leading edge separation in the diffuser and high deterministic stresses. These phase-averaged results (solid circles) are unknown during passage-averaged simulations of the flow within the stator and the rotor, and therefore they cannot be used as input into a model. However, the non-uniform outflux from the impeller can be deduced from the passage averaged simulations of the flow within the rotor. As an illustration, the solid line in Figure 10a is the angle α formed between the rotor passage-averaged velocity (Figure 9b) and the tangential direction, when this steady velocity field is rotated (as in the swept-wake model) and plotted at the same phase as the phase-averaged values. The rotor passage-averaged information (solid line) would be available during a passage-averaged simulation, therefore it can be used as input to a model. This comparison shows that sweeping the rotor passage-averaged velocity distribution appears to give a reasonably accurate indication of the time-varying inflow angle into the stator row.

5.2 Model formulation: As opposed to the swept wake model, the rotated passage-averaged field is not used directly to evaluate the deterministic stresses, but is used only as an input (boundary condition) for separate steady calculations of the flow in the stator domain. More in general, the presently introduced bimodal (or multimodal in other cases) deterministic stress model is based on performing two (or more, n) simplified steady RANS calculations of the flow inside the downstream blade-passage (B_d), for two (or more) representative phases of the upstream blades (B_u). For these simplified calculations in B_d, the computational domain D_d only covers the blade-row B_d and does not extend to include upstream and downstream blade-rows, as it does in the full passage-averaged calculation. For each calculation k (k=1,2,..,n), the inlet condition into the domain D_d is the passage-averaged velocity $v^{pass\text{-}k}(x_{in})$ from B_u, at positions x_{in}, which coincide with the inlet boundary of D_d(in this regard, and only for the purpose of estimating the deterministic stresses, the method resembles the mixing planes approach - see Section 2.1). To each such rotor outflow structure, we assign a weight w_k (k=1,2,..,n), equal to the fraction of time for which that specific the inlet condition occurs.

Suppose that each of the n simplified calculations yields a velocity field $u^k(x)$, with x pertaining to D_d and with $u^k(x_{in}) = v^{pass\text{-}k}(x_{in})$. The deterministic stresses are then evaluated as:

$$\tau_{ij}^{det} = -\frac{1}{n}\sum_{k=1,n} w_k \left(u_i^k\right)' \left(u_j^k\right)' \qquad (1)$$

where $(u_i^k)'$ is the deviation of the kth velocity field from the mean velocity over all the n simplified simulations,

$$\left(u_i^k\right)' = u_i^k(x) - \frac{1}{n}\sum_{k=1,n} w_k u_i^k(x) \qquad (2)$$

The summations approximate a time integration over a period equal to a rotor passage.

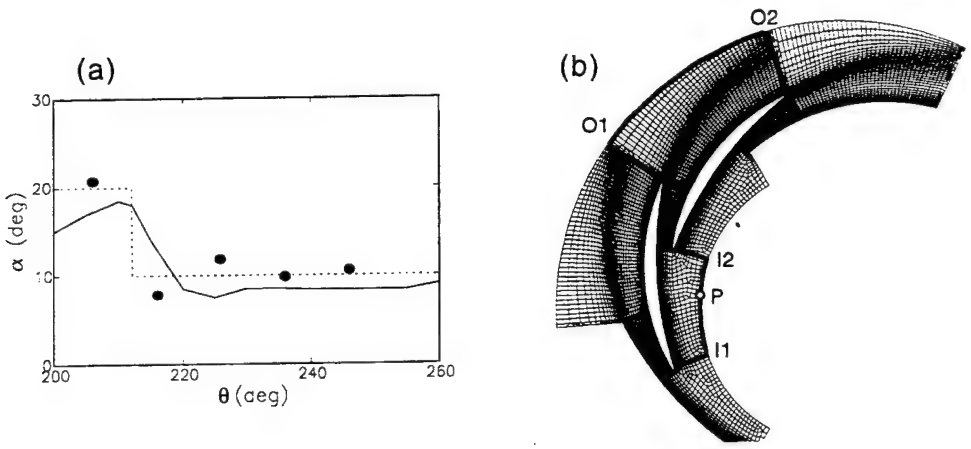

Figure 10: (a) The measured angle formed by the velocity and the tangential direction, at a point P (sown in (b)). Solid circles: Angle of the phase-averaged velocity as function of rotor phase (orientation). Solid line: angle obtained by sweeping the measured passage-averaged velocity in the rotor frame (Figure 5b) past point P, as function of angular position of the blade. Dotted line: The bimodal approximation of the variations in the orientation of the velocity used in the present analysis. (b) Mesh used in FLUENT™ calculations of flow in the stator domain. The computational domain is marked by the dark contour. Cyclic periodic boundary conditions are used, and two cyclic repetitions are shown for clarity. The inlet of the computational domain is the segment I1-I2 and the outlet is O1-O2.

5.3 Illustration of the model: To illustrate and test the approach, we choose the case shown in Fig. 10(a). In this case the upstream blade row, B_u, is the rotor blade row, and the downstream one, B_s, is the stator blade row. It appears that the cycle is reasonably well represented by two different inlet conditions (i.e. n=2). The two representative outflows from the rotor correspond (approximately) to a velocity magnitude of 2.2 m/s at an angle $\alpha_1=20^0$, and a velocity magnitude of 4.3 m/s at an angle $\alpha_2=10^0$. Notice that we are approximating the measured inlet velocity distributions shown in Figure 10a as a two-step function which is illustrated by the dotted line. Since from Fig. 10a it appears that the $\alpha_1=20^0$ flow angle occurs for about 20% of the rotor passage, the assigned weights are w_1=1/5 and w_2=4/5.

To perform the two simplified steady RANS calculations in the stator domain, we apply FLUENT™ in a 2-D domain with cyclic periodic boundary conditions. Both the standard k-ε (with wall-function) and the RNG k-ε model are used to represent turbulence effects. No significant differences in results were observed between the two turbulence models, and so only results from the RNG k-ε model are shown below. Figure 10b shows the grid utilized, including some periodic repetitions. The geometry reproduces exactly a 2-D section across the stator blade geometry of Sinha et al. (2000a, b). The mesh has a very good resolution of the near-wall and wake regions. Point P is the location at which the phase-averaged velocities (and swept passage averaged velocities), shown in Fig. 10a, are obtained. The inlet condition, i.e. a fixed velocity magnitude and a fixed α, is applied at the inlet at the segment *I1-I2* (corresponding to the set of points x_{in}). Outlet boundary conditions are applied at *O1-O2*.

The calculated velocity fields are shown in Figures 11a and 11b, for k=1 and 2, respectively. Clearly, for the k=1 case of 20^0 inlet velocity, boundary layer separation occurs at the leading edge of the stator. Conversely, the flow remains attached for the k=2, lower incidence angle (10^0) case. This "flip-flopping" between attached and separated flow around the leading edge should produce strong deterministic stresses and kinetic energy there. Figure 12 shows the modeled distribution of deterministic kinetic energy. This result should be compared with Figure 8d, which shows the experimentally measured distribution of deterministic kinetic energy. Clearly, the peak region around the leading edge, and even the peak magnitudes, are well described by this model. Similar conclusions are reached upon comparing the modeled deterministic shear stress τ_{12}^{det} distribution (not shown) with the measured one. It is encouraging that this fairly simple approach is capable of reproducing such complex effects. As noted before, these deterministic kinetic energy peaks around the stator leading edge are not tangentially uniform, and hence cannot be reproduced by a swept-wake model.

However, problems still remain in predicting the deterministic kinetic energy and shear stress levels in the stator wake, which appears to be significantly higher in the measured distributions than in the model. When we carefully compare the flow-field in Figure 11b to the phase-averaged velocity distributions at the corresponding phases, we notice that the latter display mid

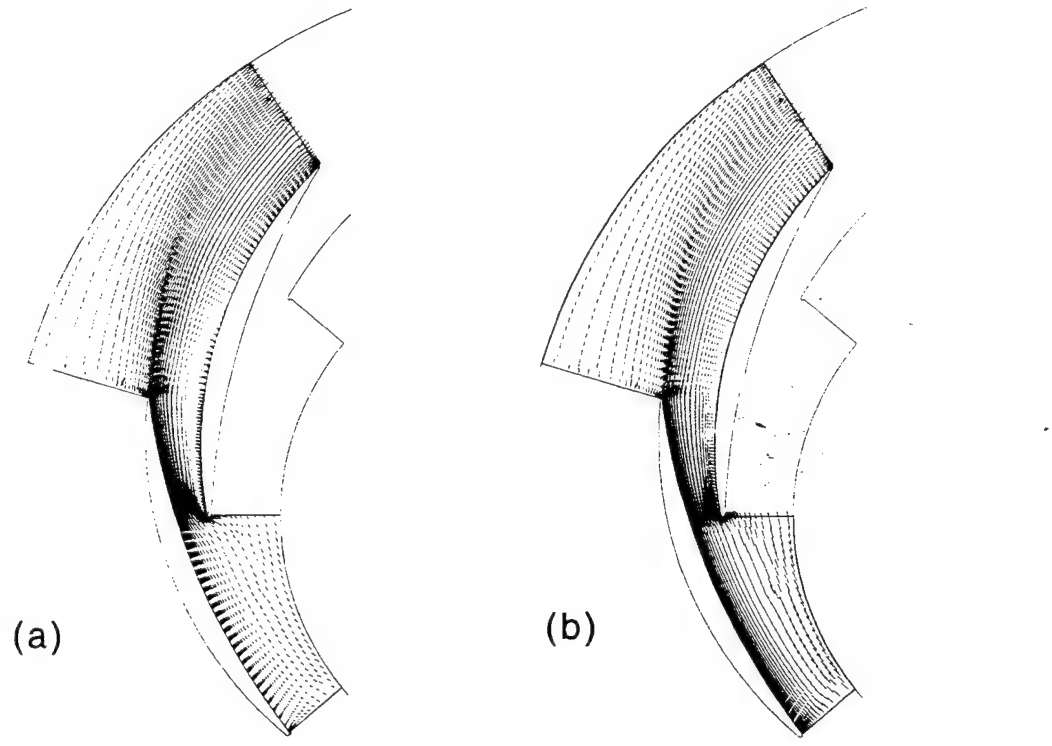

Figure 11. Velocity fields computed for different inlet conditions. (a) k=1 - the high inlet angle of 20^0 case; (b) k=2 - the low inlet angle of 10^0 case. In both cases shown the RNG k-ε model is used. Similar results are obtained using the traditional k-ε model with near-wall corrections. The flow in (a) exhibits leading edge separation, while the flow in (b) remains attached.

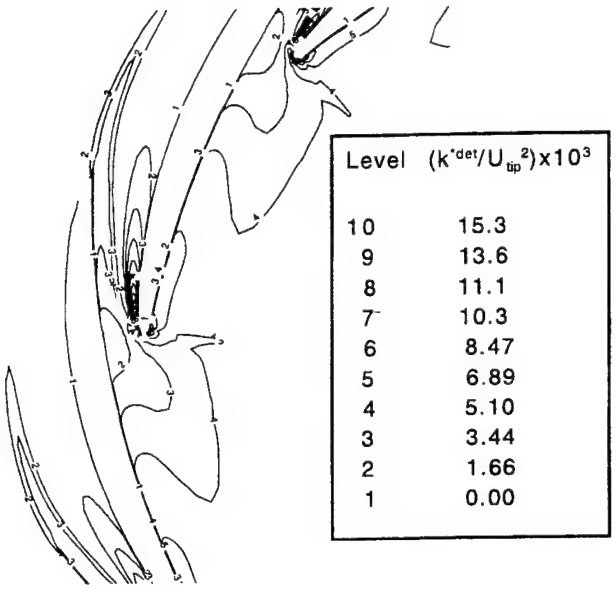

Figure 12: Deterministic kinetic energy ($-\tau_{ii}^{det}/2$), as calculated from the bimodal model. Peak values occur near the separated flow region and agree with the experimental data in Figure 4c. The values in the stator wake fall below the measured values.

vane separation on the suction side, whereas the RANS calculated field remains attached. This experimentally observed, phase-dependent mid-vane separation results in additional meandering of the wake, as compared to the calculated wake, which does not change significantly between cases k=1 and k=2. Additional work is now in progress to find out how much additional information is needed at the inlet in order to reproduce the mid-vane separation. For example, instead of specifying a constant velocity at the inlet, one can prescribe a profile that provides a better representation for the tangential variations observed in the passage-averaged velocity field. Conversely, it is also possible that the basic problem lies with the RANS turbulence modeling used, which may be insufficient to properly reproduce this effect. Clearly, more work is essential.

The practicality of the model introduced in this proposal relies on our ability to represent the entire cycle by only a few representative inlet conditions, so that only a few steady RANS calculations need to be performed. In general these calculations should be done in 3-D, but in the present example 2-D calculations are sufficient, due to the mainly 2-D nature of the phase-averaged flow in the vaned diffuser of the pump. It is unlikely that such 2-D flow would exist in the axial flow facility. Clearly, this model development is in its infancy and needs substantial additional work, refinement and further tests. Future evaluations and testing will be performed based on the present data as well as the experimental results that will be generated in the axial flow facility.

6. Subgrid modeling for Large Eddy Simulations in Turbomachines:

6.1 Background: In Large-Eddy-Simulation, spatially filtered 3-D, unsteady Navier-Stokes equations are solved. Spatial filtering of the equations creates the subgrid (SGS) stress tensor, $\tau_{ij}^{SGS}(x,t)$, defined as

$$\tau_{ij}^{SGS}(\boldsymbol{x},t) = \widetilde{u_i u_j} - \tilde{u}_i \tilde{u}_j \tag{3}$$

where "~" denotes spatial filtering at a scale Δ. Compared to RANS, in LES the mean flow variables are generally predicted with a smaller number of adjustable model coefficients. Moreover, besides improvements in mean-flow predictions, intrinsic advantages of LES exist when one is interested in higher-order quantities, such as rms and spectra of pressure fluctuations, probabilities of extreme events, instantaneous flow response to control strategies, etc. However, the unresolved scales of motion must be modeled (see e.g. Rogallo & Moin 1984, Lesieur & Metais 1996, Meneveau & Katz, 2000). The LES modeling problem consists in having to replace the subgrid stress with an expression in terms of the resolved velocity. The most commonly employed model is the traditional Smagorinsky model, given by;

$$\tau_{ij}^{smag} = -2(c_s\Delta)^2 \mid \tilde{S} \mid \tilde{S}_{ij} \tag{4}$$

where S_{ij} is the filtered strain-rate tensor. An important property of the SGS stress is its effect on the evolution of kinetic energy of the resolved scales. By deriving the transport equation for resolved kinetic energy, it is simple to show that the dissipation rate, Π(x,t) is given by:

$$\Pi(\mathbf{x},t) = -\tau_{ij}^{SGS}\tilde{S}_{ij} \tag{5}$$

Previous fundamental studies have dealt with basic properties of $\tau_{ij}(\boldsymbol{x},t)$ and Π(x,t) in simple equilibrium flows, such as isotropic turbulence (Clark et al. 1979), channel flow (Piomelli et al. 1996), jets (Liu et al. 1994), wakes (O'Neil & Meneveau 1997), etc., and in strongly distorted flows (rapid axisymmetric expansion, Liu et al. 1999).

6.2 Issues Related to SGS Modeling in turbomachines: Our present goal is to address some of the open issues for LES in the context of the highly complex flow conditions encountered in turbomachines. As an example, we present results obtained using the centrifugal pump data (Sinha et al., 2000a, b). As in Liu et al. (1994), a box-filter is employed to filter the data. We choose a filter of length Δ=6.3 mm, corresponding to three measurement grid-points. This length is the smallest scale at which we can filter the present PIV data. Since this scale is about half the stator blade thickness, it is of the same order of magnitude as the turbulence integral scale in the wake of the stator. Results of the present analysis are thus relevant to modeling for what is commonly referred to as VLES, Very Large Eddy Simulations, where only eddies with size comparable to the integral scale are resolved. The measurements that are presently in progress in the axial flow facility focus on generating data specifically for LES modeling. Consequently, we are generating will have substantially higher spatial resolution in the region of interest (at least 128x128 vectors/realization), which in some cases will be significantly smaller than the integral scale (or blade passage).

In this report we provide only a brief demonstration of issues related to LES modeling in turbomachines. Further information can be found in Sinha et al. (2000b). Figure 13a shows a sample instantaneous distribution of $\tau_{12}^{SGS}(\mathbf{x},t)$, computed from an instantaneous velocity distribution. The white area denotes regions surrounding the blades where the stress cannot be evaluated since the filter extends into the blade/vane. As is evident from this sample, the most intense events occur in the stator wakes and along the suction side of the vanes, where as noted before, the flow separates.

Next, the Smagorinsky model is evaluated from the data, as in Liu et al. (1994), using centered finite differencing for the strain-rate and a standard value c_s=0.16. Model results for the same data set shown in Figure 13a are presented in Figure 13b. Clearly, there are significant

differences between the modeled and measured stresses. Most striking is the fact that on the suction (convex) sides of the both diffuser vanes the modeled and real peaks have opposite signs. The wakes starting at the visible trailing edge have modeled and real stress with the same signs. However, the Smagorinsky model underpredicts the real stress by over one order of magnitude. This trend is consistent with previous results (Liu et al. 1995) in the far-field of a jet and in rapidly strained flow (Liu et al., 1999). The Smagorinsky model is calibrated to reproduce the correct energy dissipation rate in isotropic turbulence, but severely underpredicts the magnitude of stresses. Improved models, such as the similarity and dynamic models, will be examined from such data in forthcoming work. They are not examined with the present data because of resolution limitations. With the present data these models require filtering at sizes comparable to the width of the vane passage.

It is also instructive to evaluate the SGS dissipation. Since the PIV data provides only four out of six tensor elements, we follow the procedure of Liu et al. (1994, 1999) and approximate the full tensor contraction by assuming isotropy for the unknown elements. Thus, $\Pi(x,t)$ is approximated as:

$$\Pi(\mathbf{x},t) = -(\tfrac{1}{2}\tau_{11}^{SGS}\tilde{S}_{11} + \tfrac{1}{2}\tau_{22}^{SGS}\tilde{S}_{22} + 6\,\tau_{12}^{SGS}\tilde{S}_{12}) \tag{6}$$

Figure 14a shows an instantaneous distribution of SGS dissipation. Positive peaks appear at the stator's near-wake and at the separation point on the suction side of the vane. Negative dissipation peaks are evident in the separated shear layer (on both vanes) and along the leading edge of the vane. A negative peak in dissipation can be interpreted as "backscatter" of kinetic energy, namely that energy is fed from small to large scales. Inherently, the eddy-viscosity model cannot reproduce such a process, consistent with having modeled stresses with the wrong sign (Figs. 13a and 13b).

One may question how robust these features are from one realization to the next. Previous measurements in the jet or in isotropic turbulence (Liu et al. 1994, Liu et al. 1999) have shown that instantaneous backscatter events still yield an overall positive rate of dissipation upon averaging over many realizations. To examine this question we also present in Figure 14b phase-averaged dissipation over 100 data sets. From these statistically converged results (Sinha et al., 2000b), it is evident that the backscatter events remain at the same locations (although weaker). Thus, the backscatter in the separating shear layer is a robust phenomenon, at least at this filtering length. We can even speculate that this backscatter is related to vortex mergers (pairings) that occur in shear layers. Also, we cannot rule out the possibility that as the filter scale is reduced into the inertial range, the backscatter may disappear (again, requiring higher resolution data). However, for VLES the current filter scale is appropriate and the observations imply that a backscatter mechanism must be included in the modeling. These results, more than providing answers, indicate fundamental modeling problems in application of LES in complex flows that need attention. We plan to focus on these issues in the context of axial turbomachines using data that is being generated in the axial flow facility.

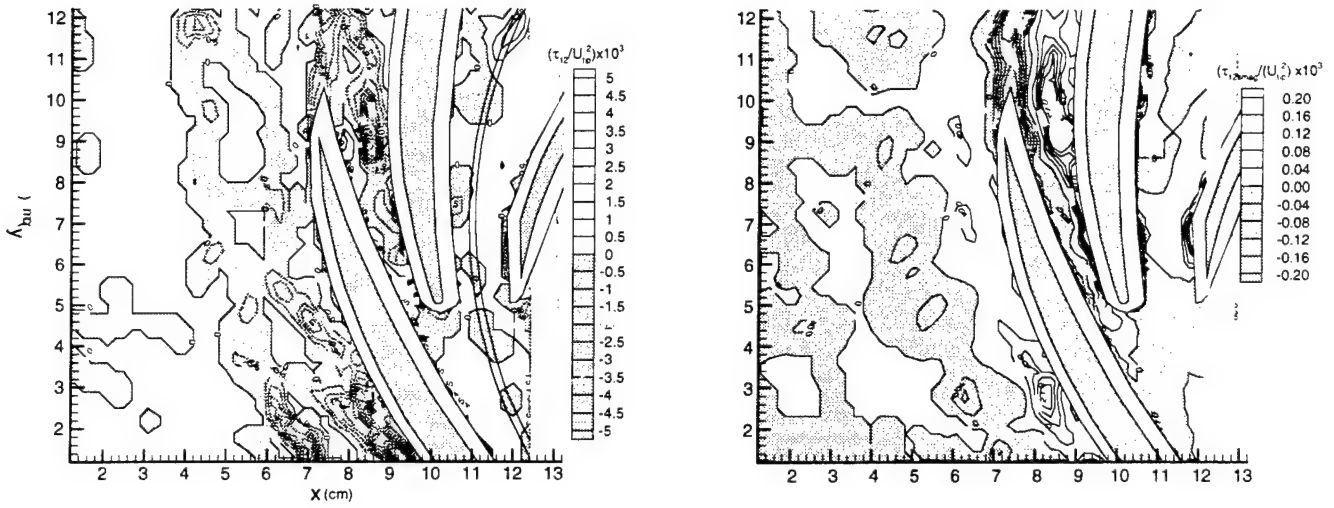

Figure 13: (a) Sample measured instantaneous distribution of SGS shear stress obtained from spatial filtering at scale Δ = 6.3mm. The phase angle is 226^0; (b) Instantaneous distribution of modeled SGS shear stress, as predicted by the Smagorinsky (eddy viscosity) model, using the filtered strain rate obtained from the same data (and same filter scale) as in (a). Note that both the magnitudes and even the signs of the modeled stresses are substantially different.

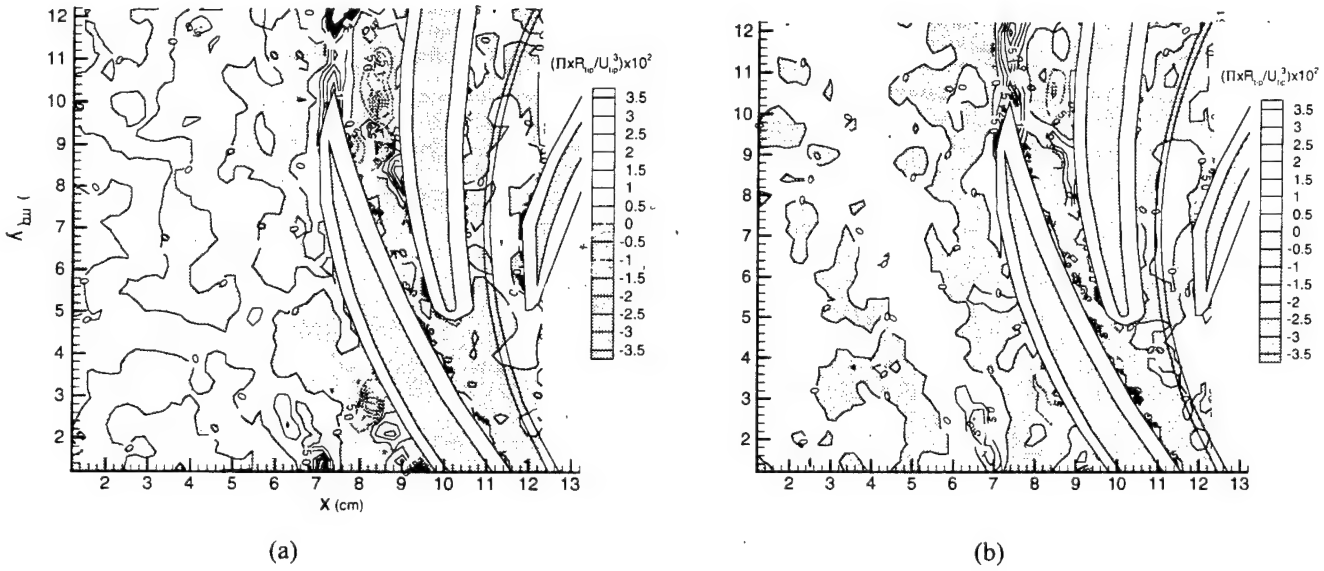

Figure 14: Distribution of SGS dissipation, Π, at the same filter scale and phase as in Figure 13. The physical interpretation of this variable (when positive) is flux of kinetic energy from large (filtered) to small (subgrid) scales. Negative values denote backscatter; (a) Instantaneous distribution for the same data used in Figure 13; (b) phase-averaged distribution determined from 100 instantaneous realizations. Note the consistent existence of a region with negative dissipation along the convex surfaces of the diffuser vanes.

7. Future Plans:

A recently awarded new AFOSR grant continues the research program summarized in this report. The effort includes detailed velocity measurements, using 2-D PIV and 3-D HPIV, as well as surface shear stress measurements within the entire (second) stage of the new, index-matched axial turbomachine facility. The data will be used for addressing turbulence-modeling issues that are relevant to flows within turbomachines, as outlined in Section 2. Specific tasks are:

a. While operating on design conditions, 2-D PIV (and selected HPIV) measurements will be performed within the rotor, stator and the gaps between them. The data will be obtained at different phases (rotor orientation relative to the stator), and repeated a sufficient number of times at the same phase, so that both the deterministic and Reynolds stresses can be determined. The spatial resolution will also be maintained at a level (typically 128x128 vectors per instantaneous realization) that will enable spatial filtering and measurements of subgrid stresses for LES. The latter will require in some cases measurements at high magnification to obtain well resolved data on small sub-sections of the flow field (e.g. a wake impacting a boundary layer).
b. Using an array of MEMS based wall shear stress sensors mounted on the surface of a stator blade, and flush mounted pressure transducers, we also plan to perform simultaneous wall stress and PIV (and selected HPIV) measurements in selected phases.
c. The data analysis includes calculations of the phase averaged velocity, pressure, and shear-stress distributions, Reynolds stresses, turbulent kinetic energy and deterministic stresses. Then, the data will be spatially filtered to obtain the filtered, large-scale flow fields and the distributions of subgrid stresses for LES.
d. In the context of passage-averaged, steady RANS, the analysis will focus on the effects of interactions between blade rows on the deterministic stresses. Included are, for example, wake, tip leakage and hub vortex interactions with downstream boundary layers, as well as boundary layer separation and "wake flutter" caused by a non-uniform velocity and pressure distributions at the exit (or entrance) from (or to) a neighboring blade row.
e. The effort to model the measured deterministic stresses will continue. For example, we will continue to evaluate a successful approach to estimate the deterministic stresses (see Section 5) that relies on steady RANS at limited, phase-dependent, non-uniform inflow conditions on the flow within a passage.
f. In the context of subgrid scale (SGS) stress modeling for LES, the measured stresses will be compared to model predictions at different scales, including eddy-viscosity, similarity and dynamic models. Specific problems, such as those related to boundary layer separation or rapid straining, will be identified and efforts will be made to propose modifications to these models that would address these problems. These efforts will be well matched with on-going efforts in much simpler configurations.
g. Still in the LES context, efforts will be made to develop models that will address the relationships between the filtered unsteady velocity field near the stator blade and the wall shear stresses. Questions as to the validity of using RANS based wall stresses as boundary conditions for LES will be addressed.

References:

Adamczyk, J.J. 1985 Model Equation For Simulating Flows In Multistage Turbomachinery. *ASME Paper No.*, 85-GT-226.

Adamczyk, J.J., Celestina, M.L., Beach, T.A., & Barnett, M. 1990 Simulation Of Three-Dimensional Viscous Flow Within A Multistage Turbine. *ASME J. Of Turbomachinery*, **112**, 370.

Adkins, G.G. & Smith, L.H. 1982 Spanwise Mixing In Axial-Flow Turbomachines. *ASME J. Of Engineering Power,* **104**, 97.

Bardina, J., Ferziger, J.H. & Reynolds, W.C 1980 Improved Subgrid Scale Models For Large Eddy Simulation, *AIAA Paper*, No. 80-1357.

Bryanston-Cross, P.J., Towers, C.E., Judge, T.R., Towers, D.P., Harasgama, S.P., Hopwood, S.T., 1992, "The Application of PIV in a Short Duration Transonic Annular Turbine Cascade," ASME J. of Turbomachinery, 114:504.

Busby J., Sondak D., Staubach B & Davis R. 2000 Deterministic Stress Modeling of a Hot Gas Segregation in a Turbine. *J. Turbomachinery* **122**, 62.

Chu, S., Dong, R. & Katz, J. 1995a Relationship Between Unsteady Flow, Pressure Fluctuations And Noise In A Centrifugal Pump. Part A: Use Of PIV Data To Compute The Pressure Field. *J. Of Fluids Engineering*, **117**, 24

Chu, S., Dong, R. & Katz, J. 1995b Relationship Between Unsteady Flow, Pressure Fluctuations And Noise In A Centrifugal Pump. Part B: Effect Of Blade-Tongue Interaction. *J. Of Fluids Eng*, **117**, 30

Clark R.A., J. H. Ferziger J.H. & Reynolds W.C., 1979 Evaluation of subgrid models using an accurately simulated turbulent flow, J. Fluid Mech . 91, 1.

Copenhaver W.W., Mayhew M.M., Hah, C. and Wadia, A.R., 1996 The effect of tip clearance on a swept transonic compressor rotor, *ASME J. Turbomachinery* **118**, 230.

Dawes, W.N. 1992 Towards improved throughflow capability: the use of three-dimensional viscous flow solvers in a multistage environment, *ASME J. of Turbomachinery* **114**, 8

Denton J.D., 1992 The calculation of three-dimensional viscous flow through multistage turbomachines *ASME J. of Turbomachinery* **114**, 18.

Dean, R.C. & Senoo, Y. 1960 Rotating Wake In Vaneless Diffusers. *J. Of Basic Engineering*, **82**, 563.

Dong, R., Chu, S., & Katz, J. 1992a, Quantitative Visualization Of The Flow Structure Within The Volute Of A Centrifugal Pump, Part A: Technique." *J. Of Fluids Eng.*, **114**, 390.

Dong, R., Chu, S., & KATZ, J. 1992b, Quantitative Visualization Of The Flow Structure Within The Volute Of A Centrifugal Pump, Part B: Results And Analysis.*J. Of Fluids Eng.*, **114**, 390.

Dong, R., Chu, S., Katz, J., (1997), "Effect of Modification to Tongue And Impeller Geometry on Unsteady Flow, Pressure Fluctuations and Noise in A Centrifugal Pump", *ASME Journal of Turbomachinery*, Vol. 119, pp. 506-515.

Dong, R., Katz, J., Huang, T.T., (1997), "On The Structure of Bow Waves on A Ship Model," *Journal of Fluid Mechanics*, Vol. 346, pp. 77-115.

Gallimore, S.J. & Cumpsty, N.A. 1986 Spanwise Mixing In Multistage Axial Flow Compressors: Part I - Experimental Investigations. *ASME J. Of Turbomachinery*, **108**, 2.

Gopalan, S., Katz, J., Knio, O., (1999) "The Flow Structure in The Near Field of Jets And Its Effect on Cavitation Inception," Journal of Fluid Mechanics, Vol. 398, pp. 1-43.

Gopalan, S., Katz, J., (1999), "Flow Structure and modeling Issues in The Closure Region of Attached Cavitation," Physics of Fluids Journal.

Gopalan, S., Liu, H.L., Katz, J., (1999), "Tip Leakage Cavitation Inception, Associated Noise and Flow Features," ASME 2000 Fluids Engineering Division Summer Meeting, June 11-15, Boston, MA, paper No. FEDSM00-11346.

Jiang, F., Tai, Y. C., Walsh, K., Tsao, T., Lee, G. B. & Ho, C. M., 1997, "A Flexible MEMS Technology and Its First Application to Shear Stress Sensor Skin," Proceedings, IEEE Micro Electro Mechanical Systems Workshop (MEMS '97), Nagoya, Japan, pp. 465-470, Jan. 26-30 (1997).

Keane, R.D., and R.J. Adrian, 1992: Theory of cross-correlation analysis of PIV images. *Applied Scientific Research*, **49**, 191-215.

Kimura, M., Tung, S., Lew, J., & Ho, C. M., 1999, "Shear Stress Imaging Micro chip for Detection of Hihg shear Stress Regions" Proceed. fo the 3rd ASMS/JSME, Joint Fluids Eng. Conf.

Kirtley, K.R., Beach, T.A., & Rogo, C. 1993 Aeroloads And Secondary Flows In A Transonic Mixed-Flow Turbine Stage. *ASME J. Of Turbomachinery*, **115**, 590.

Lakshminarayana, B. 1991 An Assessment Of Computational Fluid Dynamic Techniques In The Analysis And Design Of Turbomachinery - 1990 Freeman Scholar Lecture. *J. Of Fluids Eng*, **113**, 315.

Lejambre, C.R., Zacharias, R.M., Biederman, B.P., Gleixner, A.J., & Yetka, C.J. 1998 Development And Application Of A Multistage Navier-Stokes Solver. Part II: Application To A High Pressure Compressor Design, *ASME J. Turbomachinery* **120**, 215.

Lesieur, M. & Metais, O. 1996 New Trends In Large-Eddy Simulations Of Turbulence. *Annu. Rev. Fluid Mech.*, **28**, 45--82.

Liu, S., Meneveau, C., & Katz, J. 1994 On The Properties Of Similarity Subgrid-Scale Models As Deduced From Measurements In A Turbulent Jet. *J. Fluid Mech.*, **275**, 83.

Liu, S., Meneveau, C., & Katz, J. 1995 Experimental Study Of Similarity Subgrid-Scale Models Of Turbulence In The Far-Field Of A Jet. *Appl. Sci. Res.*, **54**, 177.

Liu, S., Katz, J. & Meneveau, C 1999 Evolution And Modeling Of Subgrid Scales During Rapid Straining Of Turbulence. J. Fluid Mech. **387**, 281.

Liu, C., Tai, Y.C., Huang, J., and Ho, C. M., 1994, "Surface-Micromachined Thermal Shear Stress Sensor," Application of Microfabrication to Fluid Mechanics, FED-Vol. 197, pp. 9-16, ASME.

Mason, P.J., 1994, "Large Eddy Simulation: a Critical Review of The Technique," *Q.J.R. Meteorol. Soc.*, 120:1.

Meneveau, C. 1993 Statistics of turbulence subgrid-scale stresses: Necessary conditions and experimental tests *Phys. Fluids A* **6** 815.

Meneveau, C. & Katz, J., 2000, Scale-invariance and turbulence modeling for Large Eddy Simulation. *Annual Rev. Fluid Mech.* **32**, 1-32.

O'Neil, J. & Meneveau, C 1997 Subgrid-Scale Stresses And Their Modeling In The Turbulent Plane Wake, *J. Fluid Mech.*, **349**, 253.

Piomelli, U. 1999 Large-eddy simulation: Achievements and challenges *Progr. Aerospace Sci.* **35**, 335.

Piomelli, U., Yu, Y. & Adrian, R. 1996 Subgrid-Scale Energy Transfer And Near-Wall Turbulence Structure, *Phys. Fluids* **8**, 215.

Rai, M.M. 1987 Navier-Stokes Simulation Of Rotor/Stator Interaction Using Patched And Overlaid Grids. *J. Of Propulsion And Power*, **3**, 387.

Rhie, C.M., Gleixner, A.J., Spear, D.A., Fischberg, C.J., & Zacharias, R.M. 1998 Development and Application Of A Multistage Navier-Stokes Solver. Part I: Multistage Modeling Using Body Forces and Deterministic Stresses. *ASME J. Turbomachinery* **120**, 205.

Rogallo, R. & Moin, P. 1984 Numerical Simulation Of Turbulent Flows. *Ann. Rev. Fluid. Mech.*, **16**, 99.

Roth, G.I., 1998: Developments in particle image velocimetry (PIV) and their application to the measurement of the flow structure and turbulence within a ship bow wave. Ph.D. Dissertation, The Johns Hopkins University, Baltimore, Maryland.

Roth, G.I., D. Hart, and J. Katz, 1995: Feasibility of using the L64720 video motion estimation processor (MEP) to increase efficiency of velocity map generation for particle Image Velocimetry (PIV), in *Laser Anemometry 1995*, edited by T.T. Huang, M. Kawahashi, and M.V. Otugen, Hilton Head, S.C.

Roth, G., Mascenik, D.T., Katz, J. (1999), "Measurements of The Flow Structure And Turbulence Within A Ship Bow Wave," Physics of Fluids Journal, Vol. 11, No. 11, pp. 3512-3523.

Roth, G., Katz, J., (2001), Five Techniques for Increasing the Speed and Accuracy of PIV Interrogation," Measurement Science and Technology Journal, Vol. 12, pp. 238-245.

Sinha, M. & Katz, J., 1998, "Flow Structure And Turbulence In A Centrifugal Pump With A Vaned Diffuser," Proceedings of ASME FEDSM98, *Paper No. FEDSM98-5129.*

Sinha, M., Katz, J., (2000), "Quantitative Visualization of The Flow in A Centrifugal Pump with Diffuser Vanes, Part A: On Flow Structure and Turbulence," Journal of Fluids Engineering, Vol. 122, No. 1, pp. 97-107.

Sinha, M., Katz, J., Meneveau, C., 1998, "Addressing Passage-Averaged And LES Modeling Issues In Turbomachinery Flows Using Two-dimensional PIV Data," Proceedings of ASME FEDSM98, *Paper No. FEDSM98-5091.*

Sinha, M., Katz, J., Meneveau, C., (2000), "Quantitative Visualization of The Flow in A Centrifugal Pump with Diffuser Vanes, Part B: Addressing Passage Averaged and LES Modeling Issues in Turbomachinery Flows," Journal of Fluids Engineering. Vol. 122, No. 1, pp. 108-116.

Sinha, M., Pinarbasi, A., Katz, J., (2001), "The Flow Structure During Onset and Developed States of Rotating Stall Within a Vaned Diffuser of a Centrifugal Pump," accepted for publication in Journal of Fluids Engineering.

Sridhar, G., Katz, J., (1995), "Lift and Drag Forces on Microscopic Bubbles Entrained by a Vortex", Physics of Fluids, Vol. 7, No. 2, pp. 389-399.

Speziale, C. 1991 Analytical methods for the development of Reynolds-stress closures in turbulence, *Ann. Rev. Fluid Mech.* **23**, 107.

Suryavamshi N, & Lakshminarayana, B. 1992 Numerical prediction of wakes in cascades and compressor rotors including the effects of mixing: Part I -cascade wakes including the effects of incidence and free-stream turbulence, *ASME J. of Turbomachinery* **114**, 607.

Tao, B., Katz, J., Meneveau, C., (1999), "Application of HPIV Data of Turbulent Duct Flow For Turbulence Modeling," Proceedings of FEDSM'99, *3rd ASME/Joint Fluids Engineering Conference*, July 18-23, San Francisco, CA, paper No. FEDSM99-7281.

Tao, B., Katz, J., Meneveau, C., (2000), "Geometry and Scale Relationships in high Reynolds Number Turbulence determined from 3-D Holographic Velocimetry," Phys. Fluids, Vol. 12, pp. 941-944.

Tao, B., Katz, J., Meneveau, C., (2000), "Effect of Strain Rate and Subgrid Dissipation Rate on Alignment Trends Between Large and Small Scales in Trubulent Duct Flows, ASME 2000 Fluids Engineering Division Summer Meeting, June 11-15, Boston, MA, paper No. FEDSM00-11164.

Tao, B., Katz, J., Meneveau, C., (2001), "Holographic PIV Measurements of the Structure of SGS Stress Eigenvectors and their alignment Relative to Parameters Based on the Filtered Velocity Gradients," submitted for publication in the Journal of Fluid Mechanics.

Tisserant, D., & Breugelmans, F.A.E., 1995, "Rotor Blade-to-Blade Measurements Using PIV, ASME *Int. Gas Turbine and Aeroengine Congress & Expo*, 95-GT-99.,

Wilcox, D.C. 1993, Turbulence Modeling for CFD (*DCW Industries, Inc.*, La Canada, CA 91011)

Zhang, J., Tao, B. & Katz, J. 1997 Turbulent Flow Measurement In A Square Duct With Hybrid Holographic PIV, *Experiments In Fluids* **23**, 373.